Available online at www.sciencedirect.com
SCIENCE DIRECT
Journal of Molecular Structure 795 (2006) 54–77
Journal of MOLECULAR STRUCTURE
www.elsevier.com/locate/molstruc

# Simultaneous analysis of rovibrational and rotational data for the $4^1$, $5^1$, $6^1$, $7^2$, $8^1$, $7^19^1$ and $9^2$ states of HCOOH

Oleg I. Baskakov [a], Igor A. Markov [a], Eugen A. Alekseev [b], Roman A. Motiyenko [b], Jarmo Lohilahti [c], Veli-Matti Horneman [c], Brenda P. Winnewisser [d,*], Ivan R. Medvedev [d], Frank C. De Lucia [d]

[a] *Department of Quantum Radiophysics, The Karazin National University, Svobody sq. 4, 61077 Kharkov, Ukraine*
[b] *Institute of Radio Astronomy of NASU, Chervonopraporna 4, 61002 Kharkov, Ukraine*
[c] *Department of Physical Sciences, University of Oulu, P.O. Box 3000, Fin 90014, Finland*
[d] *Department of Physics, The Ohio State University, 191 West Woodruff Avenue, Columbus, OH 43210, USA*

Received 19 December 2005; received in revised form 2 February 2006; accepted 3 February 2006

**Abstract**

In order to carry out an analysis of the high resolution FTIR spectrum of the $\nu_5$ vibrational band of HCOOH, it was found necessary to include in the analysis the seven interacting vibrational states $8^1$, $6^1$, $5^1$, $7^2$, $7^19^1$, $9^2$ and $4^1$. New FTIR and MMW–SMMW data, recorded with the FASSST spectrometer, and some previously published data were included in the fit. A complete set of parameters, describing the unperturbed states and the interactions, was obtained. All observed perturbations are accounted for and assignments to high quantum numbers were possible.


*Keywords:* Formic acid; Vibrational states; Interaction; Perturbation

## 1. Introduction

Studies of high resolution spectra of the fundamental vibrational bands of formic acid, HCOOH, have not until now included the $\nu_5$ or $\nu_4$ bands. In the present work, we have investigated the high resolution FTIR and millimeter and submillimeter wave (MMW–SMMW) spectra of the $5^1$ and $4^1$ states and five other states, which interact observably with these two fundamental excited states, so that now all fundamental bands except $\nu_1$ and $\nu_2$ have been studied at high resolution.

Formic acid HCOOH is a five atomic, planar molecule belonging to the $C_s$ point group. We refer in this work only to the dominant rotamer, in which the two H atoms are trans to one another. It is a nearly prolate symmetric top with asymmetry parameter $\kappa = -0.95$ which can be analyzed using Watson's effective Hamiltonian in the $I^r$ coordinate representation employing the A-reduced Hamiltonian. The investigation of the rotational and rovibrational spectra of formic acid has a long history. The microwave and millimeter-wave rotational spectrum in the ground vibrational state has been studied since the middle of the 1950s, and a full list of the resulting work before 1978 can be found in Ref. [1]. Later work extended into the SMMW [2] and FIR [3] regions. The most recent and complete investigation of the ground state was that of Winnewisser et al. [4], in which new measurements in the MMW and SMMW regions with frequencies up to 1 THz and FTIR spectra in the range 20–100 $cm^{-1}$ with a resolution 0.0012 $cm^{-1}$ were analyzed. A set of rotational parameters including quartic, sextic and some octic centrifugal distortion parameters was obtained.

HCOOH has nine normal vibrations: seven vibrations of $A'$ and two vibrations of $A''$ symmetry. A general description of the fundamental bands, taken from low resolution gas phase spectra, is given in Table 1. A good introduction to the vibrational spectrum of HCOOH is provided by the work of Redington [8], who recorded the spectra of all fundamental bands of 24 isotopic species of formic acid incorporated into low temperature Ne matrices, and evaluated a harmonic force field. The fundamental IR bands of $A'$ symmetry are a,b-hybrid bands while those of $A''$ symmetry are c-type. The majority of the excited fundamental vibrational states are perturbed to a greater or lesser extent. The two lowest vibrational states, $7^1$

* Corresponding author.
*E-mail address:* winnebp@mps.ohio-state.edu (B.P. Winnewisser).

0022-2860/$ - see front matter © 2006 Elsevier B.V. All rights reserved.
doi:10.1016/j.molstruc.2006.02.052

Table 1
Experimental frequencies and intensities of the fundamental vibrational bands of trans-formic acid

| | Mode | Wave-number[a] ($cm^{-1}$) | Integral extinction[b] (km $mol^{-1}$) | Assignment[b] |
|---|---|---|---|---|
| $A'$ | $\nu_1$ | 3570.0 | 27.2 | $\nu$ OH (100) |
| | $\nu_2$ | 2943.8 | 10.2 | $\nu$ CH (100) |
| | $\nu_3$ | 1776.2 | 81.8 | $\nu$ C=O (71), $\delta$ CH (16), $\nu$ C–O (9) |
| | $\nu_4$ | 1387.0[c] | 1.3 | $\delta$ CH (73), $\nu$ C=O (18) |
| | $\nu_5$ | 1223.0 | 5.2 | $\delta$ OH (69), $\nu$ C–O (15), $\delta$ OCO (9) |
| | $\nu_6$ | 1105.4 | 79.8 | $\delta$ C–O (65), $\delta$ OH (21), $\delta$ CH (7) |
| | $\nu_7$ | 625.4 | 21.8 | $\delta$ OCO (85) |
| $A''$ | $\nu_8$ | 1033.4 | 1.0 | $\gamma$ CH (95) |
| | $\nu_9$ | 641.8 | 56.7 | $\gamma$ OH (99) |

[a] From Ref. [5].
[b] From Ref. [6]. $\nu$, stretching vibration; $\delta$, bending vibration; $\gamma$, out-of-plane vibrations. Potential energy distribution in percent.
[c] From Ref. [7].

and $9^1$, are of different symmetries and show strong a- and b-type Coriolis coupling. Next in energy are the $8^1$ and $6^1$ states. They are also of different symmetries and also interact through a- and b-type Coriolis resonance. However, because of the larger difference of the vibrational energies, the effect of the mutual perturbation is less than in the case of the $7^1$ and $9^1$ states. For the higher fundamental excitations, the challenge becomes more complex, because the influence of overtones and combinations of the lower states becomes apparent. The analysis of the corresponding fundamental bands is therefore complicated and can be ambiguous, especially because of perturbations from dark combination and overtone states.

High resolution FTIR spectra have been obtained and analyzed up until now only for the $\nu_3$, $\nu_6$, $\nu_7$, $\nu_8$, and $\nu_9$ bands. The $\nu_1$ band was only recorded but not analyzed while the $2\nu_1$ and $3\nu_1$ overtones were fitted and rotational and centrifugal distortion parameters have been determined [9,10]. The $2\nu_2$ band has also been analyzed [10]. The most attention has been paid to the $\nu_6$ and $\nu_8$ bands centered at 1105 and 1033 $cm^{-1}$, because SMMW laser emission can be produced between rotational levels in the $6^1$ and $8^1$ states [11,12] and because the strong Q-branch of the $\nu_6$ band is used to detect formic acid in the troposphere [13]. These two bands were studied with Fourier transform spectroscopy [13–16], diode laser spectroscopy [14], Lamb dip saturation [17], and laser-radiofrequency double resonance [18] techniques. The pure rotational transitions in the $6^1$ and $8^1$ states have also been studied [19,20]. The $\nu_7$ and $\nu_9$ bands, centered at 626 and 641 $cm^{-1}$, are prime examples of bands close together, coupled by strong a- and b-type Coriolis resonances. Several FTIR studies under different resolutions [21,22] were devoted to these bands, and there are also extensive microwave and MMW rotational data for the $7^1$ and $9^1$ states [23,24]. In recent studies [16,22], where the most accurate parameters of the $6^1$, $8^1$, $7^1$ and $9^1$ states were determined, IR, MMW and SMMW transitions were included in combined fits. The $\nu_3$ band at 1776 $cm^{-1}$ was obtained via laser-Stark and diode laser spectroscopy [25], and sub-Doppler laser-Stark and FTIR spectroscopy [26].

In some studies devoted to the investigation of high resolution IR spectra of formic acid and its isotopomers the ubiquitous presence of perturbations from unobserved vibrational states was merely noted as a fact; no attempts to take them into account were undertaken, and only 'unperturbed' lines were kept in the fits [27–30]. In other work, interactions with a dark level were taken into account by means of one or two interaction terms [31–35,26]. In spite of these measures, many transitions had to be omitted from those fits.

For rovibrational bands of formic acid that are moderately intense, and for which interactions between vibrational states were taken into account completely, the number of assigned transitions has been shown to be more than 4000, and maximal values of $J$ and $K_a$ reach 70 and 20, respectively. Thus meeting these values may be taken as a criterion for an analysis, which succeeds in taking into account all significant interactions of a state or set of states of formic acid. In Refs. [16,22,36–38], where the interaction pairs $9^1$, $7^1$, and $6^1$, $8^1$ are analyzed for different isotopic analogues of HCOOH, as well as in [39], where the $3^1$, $7^15^1$ and $9^15^1$ vibrational triad for HCOOD is analyzed, this criterion is fulfilled. This criterion is taken as a standard for the present study of the $4^1$ and $5^1$ excited states and all states with which they interact.

## 2. Aims and general results

The initial goal of the present work was to investigate the high-resolution IR spectrum of the $\nu_5$ fundamental band, taking into account the influence of the nearby perturbing $7^2$, $7^19^1$ and $9^2$ vibrational states. The energies of the four states $5^1$, $7^2$, $7^19^1$, and $9^2$ are all rather close. Indeed, the $7^2$, $7^19^1$ and $9^2$ states form a close triad with very strong a- and b-type Coriolis interactions of both $7^2$ and $9^2$ with the $7^19^1$ state so that they cannot be separated. Furthermore, as Bertie and Michaelian [40] showed, the $5^1$ and $9^2$ states are in strong Fermi resonance. An anomalously high intensity of the $2\nu_9$ overtone band is one result of this interaction. This can be seen in Fig. 1, in which the spectral region around the $\nu_5$ band is shown. In the course of the present work it was found that some rotational levels of the $9^2$ state were perturbed by the relatively nearby rotational levels of the $4^1$ state, due to Fermi coupling of these two states. Therefore, the additional necessity arose to include the $\nu_4$ band into a combined analysis together with the levels of the foregoing states. At an advanced stage of the process of analyzing the measured data, when high $K_a$ transitions were included into the fit, one more interaction appeared, between the $7^2$ and $6^1$ states, which could not be neglected. In turn, since the $6^1$ state is known to interact with the $8^1$ state, we had to add into the fit all the IR lines of both of these states. These had been previously measured by Burger and analyzed by Baskakov and Demaison [16], but have been remeasured in the current investigation with higher resolution.

Thus the task ultimately came to encompass an analysis of the rotational structure of seven interacting vibrational states: $8^1$, $6^1$, $5^1$, $7^2$, $7^19^1$, $9^2$ and $4^1$. As was confirmed by the full analysis, the interactions between all these states have

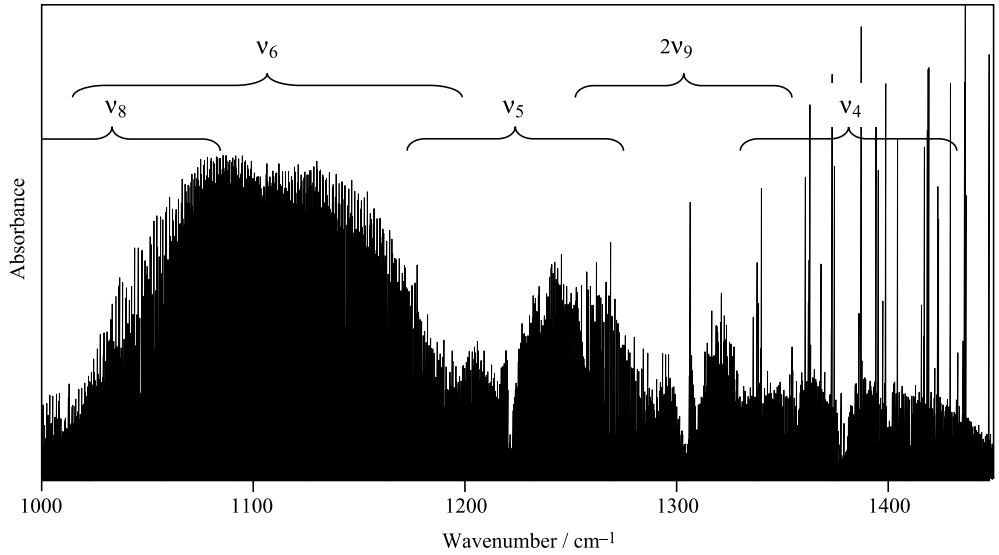


Fig. 1. Overview of the FTIR spectrum of HCOOH showing the four fundamental bands and one of the overtone bands analyzed in this study.

observable effects on the spectrum. Coriolis interactions exist not only in the $7^2/7^19^1/9^2$ triad, but also involving all of the fundamental states included: a- and b-type between the states of the different symmetry and c-type if the states are of the same symmetry. The $6^1$, $5^1$, and $4^1$ fundamental states and the doubly excited $7^2$ and $9^2$ states are connected by Fermi interactions through the cubic potential terms, and the $7^2$ and $9^2$ states are themselves coupled via the relevant quartic term in the potential energy function. Under these circumstances, an analysis of the $\nu_5$ fundamental band posed a difficult problem, especially in the initial stages, when only a limited amount of information was available. To our knowledge, a problem of such complexity has previously been solved only for lighter molecules, such as $H_2O$ or $H_2CO$, the spectrum of which is much less congested, since the number of the lines is smaller by an order of magnitude. In Fig. 2 a diagram is shown of the IR bands assigned and included into processing in the present study. Besides the $\nu_8$, $\nu_6$, $\nu_5$, $\nu_4$, $2\nu_9$, $\nu_9+\nu_7$, and $2\nu_7$ bands, we have also analyzed the hot bands $7^2\leftarrow7^1$, $7^19^1\leftarrow7^1$, $7^19^1\leftarrow9^1$, and $9^2\leftarrow9^1$ and pure rotational data for transitions in the ground and all seven $8^1$, $6^1$, $5^1$, $7^2$, $7^19^1$, $9^2$, and $4^1$ vibrational states. A summary is given in Tables 2 and 3 of the transitions assigned and those used in the fit, including the RMS deviations obtained.

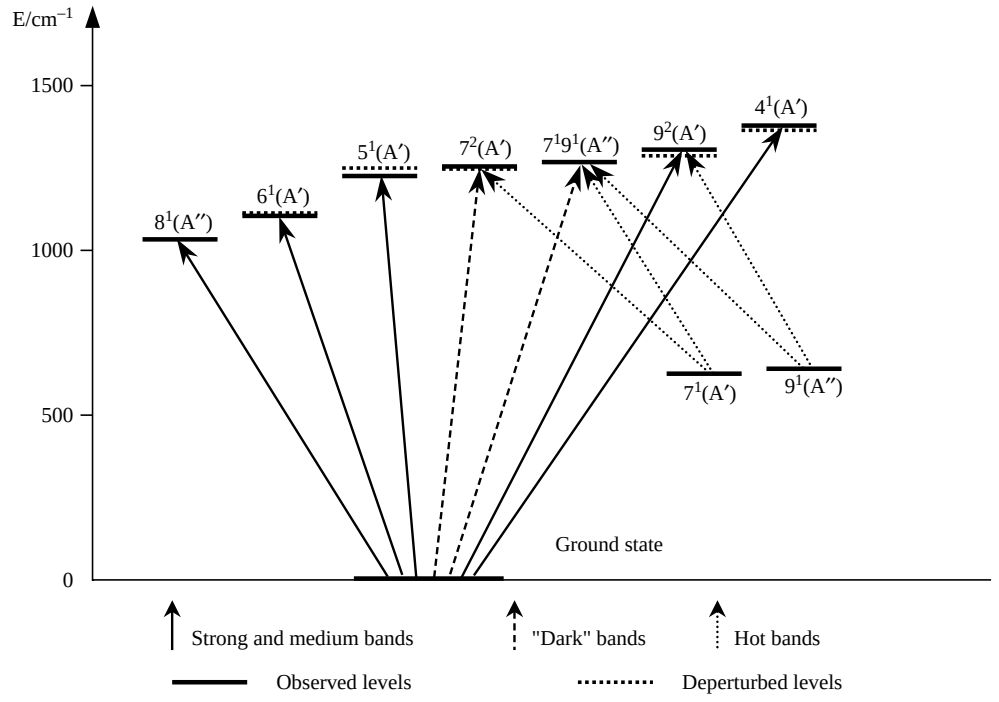


Fig. 2. Energy level diagram showing the seven interacting vibrational states of HCOOH included in this analysis. The arrows indicate observed bands included. Both observed and deperturbed band center values resulting from the analysis are shown. The lower states of the relevant hot bands assigned as part of this work are also shown.

Table 2
Summary of IR transitions of HCOOH assigned and analyzed in this work

| IR band | Number of transitions[a] | RMS deviation ($cm^{-1}$) | Max $J$ | Max $K_a$ |
|---|---|---|---|---|
| $8^1 \leftarrow gs$ | 2374 | 0.00030 | 42 | 18 |
| $6^1 \leftarrow gs$ | 7108 | 0.00024 | 76 | 22 |
| $5^1 \leftarrow gs$ | 5544 | 0.00026 | 73 | 19 |
| $7^2 \leftarrow gs$ | 1118 | 0.00037 | 46 | 19 |
| $7^1 9^1 \leftarrow gs$ | 1840 | 0.00032 | 50 | 18 |
| $9^2 \leftarrow gs$ | 3709 | 0.00028 | 57 | 19 |
| $4^1 \leftarrow gs$ | 3924 | 0.00027 | 57 | 19 |
| $7^2 \leftarrow 7^1$ | 328[b] | – | 34 | 14 |
| $9^2 \leftarrow 9^1$ | 538[b] | – | 40 | 13 |
| $7^1 9^1 \leftarrow 7^1$ | 423[b] | – | 31 | 13 |
| $7^1 9^1 \leftarrow 9^1$ | 513[b] | – | 37 | 12 |

[a] Only one component of each asymmetric doublet was counted.
[b] Hot band transitions were not used in the fit.

The final results of the complete analysis, including deperturbed band origins, rotational and centrifugal distortion parameters and all interaction parameters determined in the present work, are given in Tables 4 and 5. The reduced rotational levels of all seven vibrational states as a function of $J$, calculated with these parameters, are shown in Figs. 3 and 4. The arbitrary reference energy was chosen close to the band origin of the $\nu_5$ band. The left panel in both figures contains the levels of overall rovibrational symmetry $A'$ (E+ and O− Wang matrix levels, for which the rotational quantum numbers fulfill the rule $K_a+K_c-J=0$ if $K_a$ is even and $K_a+K_c-J=1$ if $K_a$ is odd for vibrational states of $A'$ symmetry, and E− and O+ Wang matrix levels, for which $K_a+K_c-J=0$ if $K_a$ is odd and $K_a+K_c-J=1$ if $K_a$ is even for vibrational states of $A''$). The right panel shows the levels of $A''$ symmetry (relations between rotational quantum numbers are opposite to those for $A'$ symmetry levels).

The rovibrational levels can be roughly separated onto three regions. The lowest region, which would fall in a region of negative reduced energies, contains only the low $K_a$ levels of the $6^1$ and $8^1$ vibrational states. The levels of these two states lie far apart and do not cross each other. Since this is the least informative part of the diagram, it is not shown. The middle region, between 0 and 200 $cm^{-1}$, shown in Fig. 3, contains the origins of the rotational level series of the other five vibrational states. It also contains the largest number of local perturbations caused by level crossings. In this range of reduced energy the appearance of the levels of $A'$ and $A''$ symmetry is significantly different. The third region, showing Fig. 4, stretches up above 200 $cm^{-1}$. It covers levels with relatively high $K_a$. These levels do not appear to intersect. However, due to interactions for which the magnitude generally increases with $J$ and/or $K_a$, the series are shifted and their interactions are global in nature, affecting a wide range of $J$ values. Accounting for interactions in this region allowed us to assign and include in the fit rotational levels with higher $K_a$, in particular those for the $8^1$ and $6^1$ states, than was possible in Ref. [16]. In this region the appearance of the $A'$ and $A''$ panels does not noticeably differ. This is explained by the fact that for large $K_a$ the asymmetric splitting becomes negligibly small.

This summary of the results of the analysis will be referred to in the following sections in discussing the assignment and the analysis leading to the parameters presented in Tables 4 and 5. The summary is particularly essential for the description and clarification of the observed perturbations in the spectrum.

Table 3
Summary of MMW–SMMW transitions of HCOOH assigned and analyzed in this work

| State | Number of transitions[a] | | RMS deviation (kHz) | | Max $J$ | Max $K_a$ |
|---|---|---|---|---|---|---|
| | Ohio | Kharkov | Ohio | Kharkov | | |
| gs | 619 | 48 | 33 | 8 | 70 | 14 |
| gs (total) | 934 | | 44 | | 70 | 19 |
| $8^1$ | 227 | 30 | 43 | 8 | 39 | 15 |
| $6^1$ | 204 | 32 | 47 | 13 | 29 | 13 |
| $5^1$ | 223 | 32 | 42 | 15 | 28 | 15 |
| $7^2$ | 173 | 29 | 53 | 22 | 26 | 15 |
| $7^1 9^1$ | 161 | 31 | 48 | 24 | 18 | 14 |
| $9^2$ | 180 | 32 | 46 | 16 | 27 | 14 |
| $4^1$ | 174 | 25 | 47 | 26 | 24 | 13 |

[a] Only one component of each asymmetric doublet was counted.

## 3. Experimental aspects

The experimental data used were measured in several laboratories.

The high resolution FTIR spectrum of HCOOH in the region 850–1500 $cm^{-1}$ was recorded with the Bruker IFS 120HR spectrometer in the Infrared Laboratory at the University of Oulu. The spectrometer was equipped with a Globar source, a KBr beam splitter, and a MCT detector. Altogether three measurements were made, in each of which the absorption path length was 3.2 m, but the gas pressures were varied according to the bands in each region (0.01, 0.2, and 0.9 Torr (0.0013, 0.027, 0.12 kPa) for the $\nu_6/\nu_8$, $\nu_5$, and 1300–1500 $cm^{-1}$ regions, respectively). In the $\nu_6/\nu_8$ region (1100 $cm^{-1}$) an aperture of diameter 1.3 mm was used and the recording time was 52 h. The achieved signal to noise ratio was about 300 and a line width of 0.0025 $cm^{-1}$ for weak lines was observed. The $\nu_5$ fundamental (1220 $cm^{-1}$) region and the overtone and $\nu_4$ region (1300–1500 $cm^{-1}$) were recorded with a 1.5 mm aperture and a different filter than the $\nu_6/\nu_8$ region, and the measuring time was 26 h in both of those recordings. The $S/N$ and observed line widths in these two measurements were 180 and 0.0029 $cm^{-1}$, respectively. The sample was at room temperature in an optimized White cell with KBr windows [41,42]. The calibration was based on the water lines of Ref. [43], whose systematic error was taken into account [44]. The present FTIR measurement of the $\nu_6/\nu_8$ bands was combined with the spectrum of these bands recorded under higher pressure and less overall resolution in Wuppertal and previously used in [16]. Many strong lines in the old spectrum were saturated, but many weak lines not observed in the present measurements were clearly visible. We therefore used in the fit all transitions which could be assigned in the new spectrum and all other weak transitions from the old one.

Table 4
Diagonal parameters of the ground and seven excited vibrational states of HCOOH

| | Ground state | | $8^1$ | $6^1$ | $5^1$ | $7^2$ | $7^19^1$ | $9^2$ | $4^1$ |
|---|---|---|---|---|---|---|---|---|---|
| | Ref. [4] | Present work | | | | | | | |
| $\nu_0$ ($cm^{-1}$) | | | **1033.46996***5(6)* | **1109.***20352(11)* | **1248.***66903(35)* | **1249.***00857(11)* | **1268.68926***1(5)* | **1288.***44504(44)* | **1368.***99460(14)* |
| $A$ (MHz) | **77,512.23***55(11)* | **77,512.229***90(70)* | **780,***44.9053(20)* | **77,80***3.2587(20)* | **76,6***91.6484(26)* | **77,97***5.1893(59)* | **78,05***6.6774(73)* | **77,88***5.0258(94)* | **77,1***63.7557(21)* |
| $B$ (MHz) | **12,055.106***45(19)* | **12,055.105***39(12)* | **12,063.***27354(90)* | **12,016.***52653(24)* | **11,984.***88930(81)* | **12,064.***53257(41)* | **11,928.***07216(46)* | **11,966.***44016(39)* | **12,092.***02100(24)* |
| $C$ (MHz) | **10,416.115***12(19)* | **10,416.114***59(11)* | **10,418.7***6620(19)* | **10,416.***37763(52)* | **10,393.***06769(37)* | **10,308.***13595(52)* | **10,380.1***3473(33)* | **10,401.***25751(30)* | **10,389.***85595(32)* |
| $\Delta_J$ (kHz) | **9.996***03(23)* | **9.994***62(15)* | **9.47***692(72)* | **9.6***4213(10)* | **10.23***904(64)* | **10.6***4966(10)* | **9.82***620(86)* | **10.26***630(83)* | **9.60***582(52)* |
| $\Delta_{JK}$ (kHz) | **−86.24***86(20)* | **−86.21***76(17)* | **−75.***9409(19)* | **−104.***6235(27)* | **−90.***8243(51)* | **−37.***0319(61)* | **−114.***7506(63)* | **−106.***2709(54)* | **−74.***5341(30)* |
| $\Delta_K$ (kHz) | **1702.4***47(15)* | **1702.2***92(10)* | **150***1.414(61)* | **151***4.449(58)* | **18***55.379(11)* | **208***9.065(66)* | **177***5.336(63)* | **16***82.311(11)* | **173***6.382(67)* |
| $\delta_J$ (kHz) | **1.9488***15(32)* | **1.9485***85(22)* | **1.66***9886(38)* | **2.23***1628(52)* | **1.80***1105(43)* | **1.94***4442(83)* | **1.92***1273(44)* | **1.76***1706(47)* | **2.27***8359(41)* |
| $\delta_K$ (kHz) | **42.73***18(48)* | **42.77***39(30)* | **29.***20879(30)* | *−8.28462(12)* | **62.***3534(51)* | **128.***8076(84)* | **31.***29153(70)* | **25.***04190(44)* | **24.***51522(53)* |
| $\Phi_J$ (Hz) | **0.0131***43(97)* | **0.0130***07(78)* | | **0.037***792(45)* | **0.017***984(72)* | | **0.05***6306(14)* | | **0.02***7276(31)* |
| $\Phi_{JK}$ (Hz) | **0.10***21(60)* | **0.10***11(32)* | **0.4***808(15)* | **2.4***894(78)* | **−1.7***334(26)* | **0.2***824(39)* | | | **0.1***815(14)* |
| $\Phi_{KJ}$ (Hz) | **−10.5***65(23)* | **−10.5***34(14)* | **−17.***806(21)* | | **16.***830(77)* | **−54.***118(67)* | | **−1***6.318(10)* | **−16.***327(35)* |
| $\Phi_K$ (Hz) | **121.1***95(76)* | **120.5***90(77)* | **18***4.322(37)* | **6***5.709(24)* | | **51***6.704(46)* | | | **13***6.874(17)* |
| $\phi_J$ (Hz) | **0.0057***63(12)* | **0.0057***43(13)* | | **0.018***222(20)* | **0.006***093(45)* | **−0.00***7693(11)* | **0.010***201(84)* | | |
| $\phi_{JK}$ (Hz) | **0.09***75(32)* | **0.11***36(35)* | **−1.7***059(47)* | **3.3***188(64)* | | **1.***4094(13)* | **2.***6742(13)* | | |
| $\phi_K$ (Hz) | **14.***82(33)* | **13.***87(17)* | | **17***0.93(43)* | | | | | |
| $L_J$ (mHz) | **−0.00007***19(93)* | **−0.0000***99(11)* | | | | | | | |
| $L_{JJK}$ (mHz) | | | | | | | | | |
| $L_{JJKK}$ (mHz) | **−0.03***97(56)* | **0.29***25(67)* | | | | | | | **1.8***492(92)* |
| $L_{JKKK}$ (mHz) | **0.8***75(34)* | | | | | | | | |
| $L_K$ (mHz) | **−11.***82(11)* | **−10.***57(17)* | | | | **−9***5.12(41)* | | | **−1***3.69(26)* |
| $l_J$ (mHz) | | | | | | | | | |
| $l_{JK}$ (mHz) | | **−0.003***72(40)* | | | | | | | |
| $l_{KJ}$ (mHz) | | **0.1***16(16)* | | | | | | | |
| $l_K$ (mHz) | | **11.***11(24)* | | | | | | | |

Numbers in brackets quote one standard deviation in the two first figures of the part of the parameters given in italic font.

Table 5
Off-diagonal parameters coupling seven excited vibrational states of HCOOH

| | n | q | r | s | Parameter | |
|---|---|---|---|---|---|---|
| $5^1$–$7^2$ | | | | | | |
| | 0 | 0 | 0 | + | −**2.4***178(62)* | $cm^{-1}$ |
| | 0 | 0 | 2 | + | **2.1***422(90)* | MHz |
| $5^1$–$9^2$ | | | | | | |
| | 0 | 0 | 0 | + | **41.***5344(13)* | $cm^{-1}$ |
| | 0 | 0 | 1 | − | **11***88.130(19)* | MHz |
| | 1 | 0 | 0 | + | **16.***257(25)* | MHz |
| | 0 | 0 | 2 | + | **8.***399(12)* | MHz |
| | 0 | 0 | 3 | − | **0.029***93(52)* | MHz |
| $5^1$–$4^1$ | | | | | | |
| | 0 | 0 | 1 | − | **29***24.645(32)* | MHz |
| | 0 | 2 | 0 | + | **73***4.230(40)* | MHz |
| | 0 | 0 | 2 | + | **4.***1504(16)* | MHz |
| | 0 | 0 | 3 | − | **0.05***848(11)* | MHz |
| $5^1$–$6^1$ | | | | | | |
| | 0 | 0 | 1 | − | **14***11.930(29)* | MHz |
| | 0 | 2 | 0 | + | −**3***60.391(12)* | MHz |
| | 0 | 0 | 2 | + | **2.0***783(87)* | MHz |
| | 0 | 0 | 3 | − | −**0.069***14(52)* | MHz |
| | 0 | 0 | 4 | + | **0.24***52(57)* | kHz |
| | 1 | 0 | 3 | − | **1.***782(12)* | Hz |
| | 0 | 0 | 5 | − | **0.6***36(40)* | Hz |
| $5^1$–$7^1 9^1$ | | | | | | |
| | 0 | 1 | 0 | + | **24***,175.992(23)* | MHz |
| | 0 | 0 | 1 | + | **18***89.738(22)* | MHz |
| | 0 | 0 | 2 | − | −**3.***2872(12)* | MHz |
| | 0 | 3 | 0 | + | **6.***0455(28)* | MHz |
| | 0 | 0 | 4 | − | −**0.02***558(21)* | kHz |
| | 0 | 5 | 0 | + | −**4.***1239(32)* | kHz |
| | 0 | 0 | 5 | + | −**0.3***34(21)* | Hz |
| $5^1$–$8^1$ | | | | | | |
| | 0 | 1 | 0 | + | −**84***,821.784(77)* | MHz |
| | 0 | 0 | 1 | + | −**92***67.272(79)* | MHz |
| $7^2$–$9^2$ | | | | | | |
| | 0 | 0 | 1 | − | −**16***8.4761(83)* | MHz |
| | 0 | 2 | 0 | + | **42***8.345(67)* | MHz |
| | 0 | 0 | 2 | + | −**2.6***395(88)* | MHz |
| $7^2$–$4^1$ | | | | | | |
| | 0 | 0 | 1 | − | −**5***10.218(22)* | MHz |
| | 0 | 0 | 3 | − | −**2.4***988(48)* | MHz |
| $7^2$–$8^1$ | | | | | | |
| | 0 | 1 | 0 | + | **24***99.526(25)* | MHz |
| | 0 | 0 | 1 | + | **5***87.968(42)* | MHz |
| | 0 | 0 | 3 | + | **0.010***692(80)* | MHz |
| $9^2$–$4^1$ | | | | | | |
| | 0 | 0 | 0 | + | **27.***8987(16)* | $cm^{-1}$ |
| | 1 | 0 | 0 | + | **21.***229(30)* | MHz |
| | 0 | 2 | 0 | + | −**32***4.678(10)* | MHz |
| | 0 | 0 | 3 | − | −*0.02989(41)* | MHz |
| | 1 | 0 | 2 | + | **0.39***778(56)* | kHz |
| | 1 | 0 | 3 | − | −**1.0***579(84)* | Hz |
| $9^2$–$6^1$ | | | | | | |
| | 0 | 2 | 0 | + | **7***60.678(13)* | MHz |
| | 0 | 0 | 2 | + | −**2.9***060(86)* | MHz |
| | 0 | 0 | 3 | − | −**0.02***400(13)* | MHz |
| | 0 | 1 | 3 | + | **1.3***185(96)* | kHz |
| | 0 | 0 | 4 | + | −**0.04***869(81)* | kHz |
| | 1 | 0 | 3 | − | **3.***5196(17)* | Hz |
| | 0 | 2 | 3 | − | −**0.11***285(59)* | kHz |
| $9^2$–$7^1 9^1$ | | | | | | |
| | 0 | 1 | 0 | + | −**35***,624.835(17)* | MHz |
| | 0 | 0 | 1 | + | −**45***18.722(12)* | MHz |
| | 0 | 0 | 2 | − | **7.***3798(20)* | MHz |
| | 1 | 1 | 0 | + | −**0.17***809(60)* | MHz |
| | 0 | 3 | 0 | + | **4.***4979(13)* | MHz |
| | 1 | 0 | 1 | + | **0.008***639(62)* | MHz |
| | 0 | 0 | 3 | + | **0.004***775(24)* | MHz |
| | 0 | 0 | 4 | − | −**0.06***680(49)* | kHz |
| | 0 | 5 | 0 | + | −**1.***4009(24)* | kHz |
| $9^2$–$8^1$ | | | | | | |
| | 0 | 0 | 4 | − | **0.0***5791(13)* | kHz |
| $4^1$–$6^1$ | | | | | | |
| | 0 | 0 | 3 | − | −**0.02***223(21)* | MHz |
| | 0 | 0 | 7 | − | **0.34***7(40)* | mHz |
| $4^1$–$7^1 9^1$ | | | | | | |
| | 0 | 1 | 0 | + | **14***,133.549(18)* | MHz |
| | 0 | 0 | 1 | + | **1***35.599(21)* | MHz |
| | 1 | 0 | 1 | + | **0.055***51(90)* | MHz |
| | 0 | 0 | 4 | − | −**0.3***253(17)* | kHz |
| | 0 | 1 | 4 | + | *9.1671(13)* | (Hz |
| $7^2$–$6^1$ | | | | | | |
| | 0 | 0 | 0 | + | −**25.***0420(30)* | $cm^{-1}$ |
| | 0 | 0 | 1 | − | **87***24.118(27)* | MHz |
| | 0 | 0 | 2 | + | −**14.***7960(37)* | MHz |
| | 0 | 0 | 3 | − | **0.02***688(10)* | MHz |
| | 1 | 0 | 2 | + | **0.11***44(72)* | kHz |
| | 0 | 2 | 2 | + | −**7.***225(78)* | kHz |
| | 0 | 0 | 4 | + | −**0.40***95(55)* | kHz |
| | 0 | 0 | 5 | − | −**0.2***001(26)* | Hz |
| $7^2$–$7^1 9^1$ | | | | | | |
| | 0 | 1 | 0 | + | **48***,800.459(12)* | MHz |
| | 0 | 0 | 1 | + | **73***15.792(14)* | MHz |
| | 0 | 0 | 2 | − | −**9.***1432(12)* | MHz |
| | 0 | 3 | 0 | + | −**3.***1327(11)* | MHz |
| | 1 | 0 | 1 | + | −**0.15***769(78)* | MHz |
| | 0 | 2 | 1 | + | −**7.***6096(40)* | MHz |
| | 0 | 1 | 2 | + | **0.14***42(64)* | MHz |
| | 0 | 0 | 3 | + | **0.088***26(64)* | MHz |
| | 1 | 0 | 2 | − | **0.07***380(92)* | kHz |
| | 0 | 2 | 2 | − | **0.***6577(19)* | kHz |
| | 2 | 0 | 1 | + | −**0.1***856(52)* | Hz |
| | 0 | 4 | 1 | + | **2.3***582(74)* | kHz |
| | 1 | 0 | 3 | + | **0.6***478(51)* | Hz |
| | 0 | 2 | 3 | + | **5***4.65(47)* | Hz |
| $4^1$–$8^1$ | | | | | | |
| | 0 | 1 | 0 | + | **3***4,791.138(28)* | MHz |
| | 0 | 0 | 1 | + | **15***46.350(62)* | MHz |
| | 0 | 0 | 5 | + | **5.***4905(15)* | Hz |
| $6^1$–$7^1 9^1$ | | | | | | |
| | 0 | 1 | 0 | + | −**15***,852.507(38)* | MHz |
| | 0 | 0 | 1 | + | **23***10.826(31)* | MHz |
| | 0 | 3 | 0 | + | −**12.***1060(32)* | MHz |
| | 0 | 0 | 3 | + | −**0.02***697(12)* | MHz |
| $6^1$–$8^1$ | | | | | | |
| | 0 | 1 | 0 | + | **11***,305.498(13)* | MHz |
| | 0 | 0 | 1 | + | **15***03.128(10)* | MHz |
| | 1 | 1 | 0 | + | **1.13***229(78)* | MHz |
| | 0 | 3 | 0 | + | −**2.***2134(16)* | MHz |
| | 1 | 0 | 1 | + | **0.013***40(68)* | MHz |
| | 0 | 0 | 3 | + | **0.038***48(37)* | MHz |
| | 0 | 0 | 4 | − | −**0.05***597(20)* | kHz |
| | 2 | 1 | 0 | + | −**0.01***5625(11)* | kHz |
| | 1 | 0 | 3 | + | −**4.8***084(62)* | Hz |
| | 0 | 0 | 5 | + | −**1.1***985(38)* | Hz |
| $7^1 9^1$–$8^1$ | | | | | | |
| | 0 | 0 | 1 | − | **4***11.850(36)* | MHz |

Numbers in brackets quote one standard deviation in the two first figures of the part of the parameters given in italic font. *n*,*q*,*r* are the powers of angular momenta operators defined in expression (2). Column *s* shows sign in the $\hat{J}_+^r \pm \hat{J}_-^r$ term in (2).

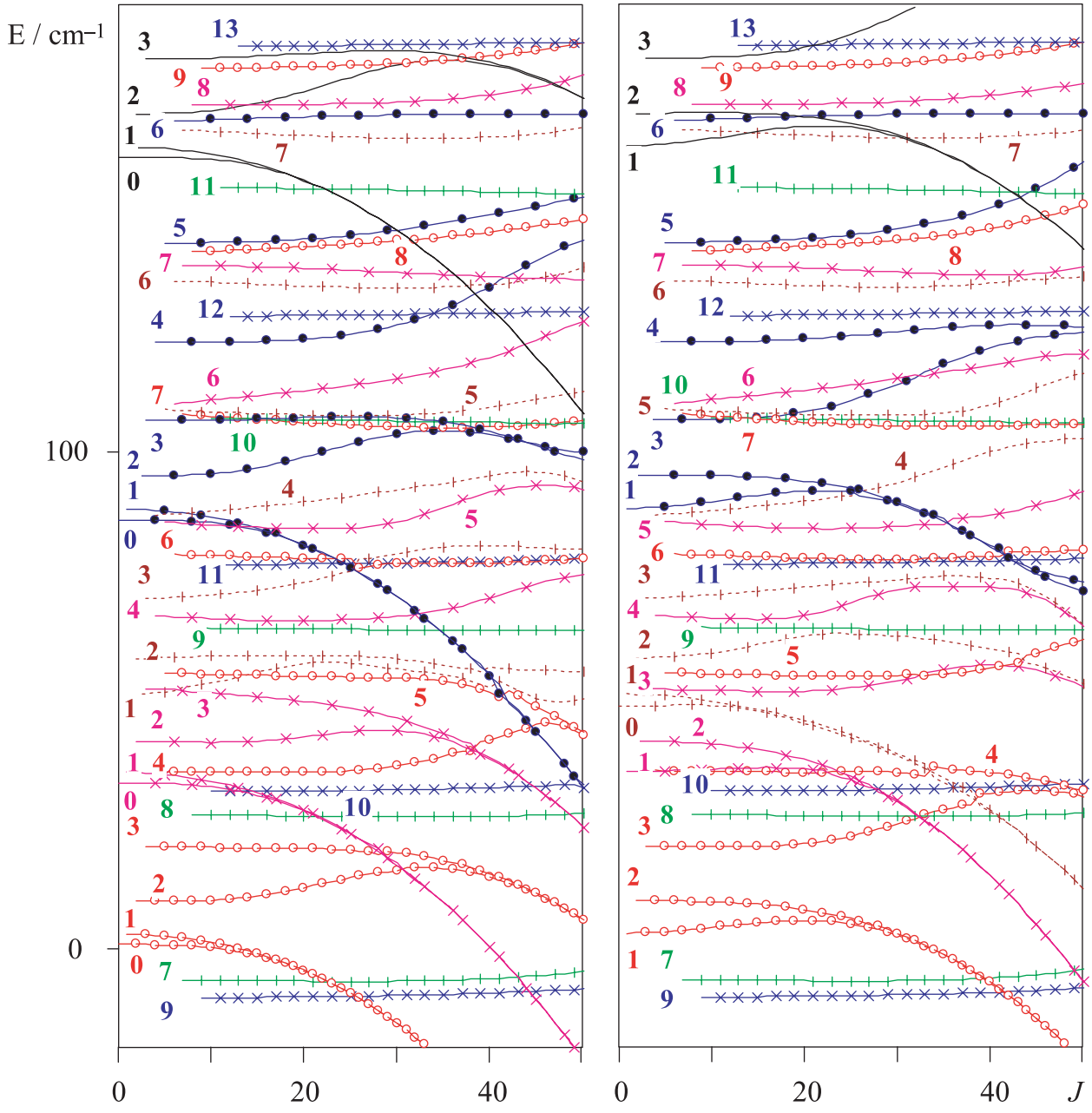


Fig. 3. Reduced rotational energies (lower part) of seven interacting states of HCOOH plotted versus $J$. The numbers indicate the value of $K_a$ for each curve. The left panel contains the levels of $A'$ symmetry and the right panel contains the levels of $A''$ symmetry. The vibrational state is indicated by the following legend

.

The transitions of the hot bands $9^2 \leftarrow 9^1$, $7^2 \leftarrow 7^1$, $9^1 7^1 \leftarrow 9^1$, and $9^1 7^1 \leftarrow 7^1$ were taken from a Fourier transform spectrum of the region 430–725 $cm^{-1}$ measured at the Justus Liebig University Giessen. The sample gas was in a 1 m White cell, set for a path length of 3.02 m, with CsI windows, at 0.062 mbar (6.2 hPa) and at room temperature. The parameters of the measurement were 1/MOPD = 0.0044 $cm^{-1}$; scanner velocity 1.266 cm/s; detector Ge:Cu; beam-splitter 3.5 μ Mylar; 7 scans; boxcar apodization. The Doppler linewidth in this region is about 0.0012 $cm^{-1}$, the pressure-broadening contribution was negligible, and the instrumental line width (FWHM) was 0.0026 $cm^{-1}$. The observed linewidth (FWHM), 0.0027 $cm^{-1}$, is consistent with these parameters.

Millimeter-wave rotational transitions in the 86–229 GHz range belonging to the vibrational states investigated here were measured using the high-precision spectrometer at the Kharkov

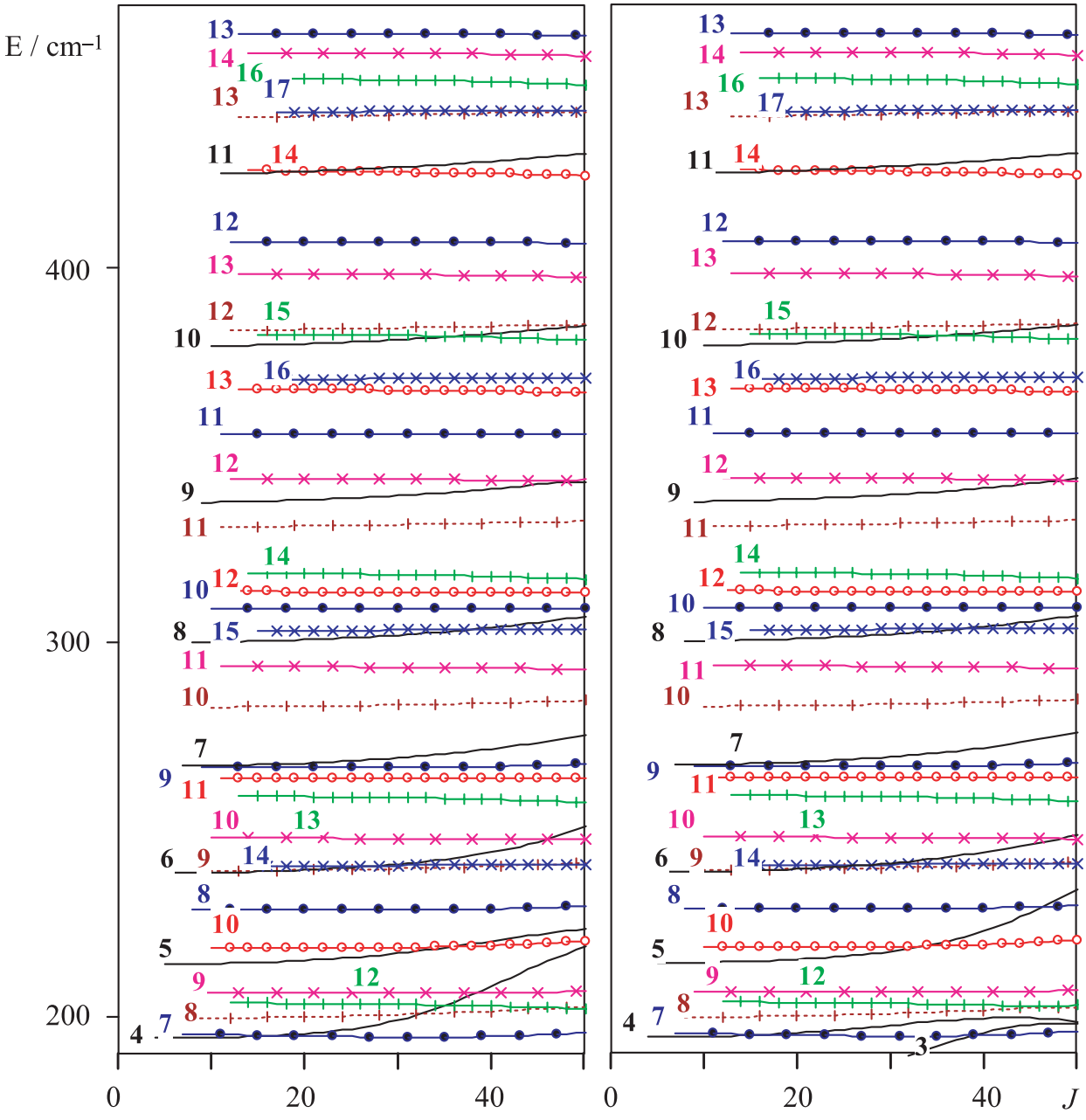


Fig. 4. Reduced rotational energies (upper part) of seven interacting states of HCOOH plotted versus $J$ (see caption of Fig. 3).

Laboratory of Molecular Spectroscopy. A brief description of the spectrometer can be found in Ref. [45]. The spectrum was observed at room temperature. The estimated experimental uncertainty for the measured transitions is assumed to be 50 kHz. This uncertainty is mainly caused by the weakness of the signals and uncertainty in pressure. For the states discussed here 387 transitions were measured.

A broad-band millimeter wave spectrum of HCOOH was obtained with the FASSST spectrometer at The Ohio State University [46–48]. The spectrum was measured at room temperature, and also at 443 K (170 °C), in a 6 m aluminum cell. Sample pressures were between 1 and 10 mTorr, with 5–15 mTorr of $SO_2$ in a separate cell in series with the sample cell, for calibration. These pressures were maintained in a slow flow. Since the achievable $S/N$ is greater than the dynamic range of the ADC employed, the room temperature spectrum was recorded at two different amplifications, allowing both strong and weak transitions to be observed without saturation due to amplification. All of the transitions used in the present work were taken from the heated sample, recorded at the higher amplification. Three BWOs were scanned, giving full coverage from 115 to 370 GHz, with a small gap from 186 to 193 GHz. The measurements incorporated improvements in FASSST data acquisition and calibration implemented recently [49,50]. Each BWO was scanned 200 times up and 200 times down in frequency. Each scan was checked for consistency and calibrated individually, and between 177 and 200 scans were retained in the various

segments. The calibration included a correction for the effect of atmospheric water on the etalon spacing affected by water lines above 250 GHz, and the up and down scans were summed separately. Line positions from the two summed spectra were then averaged. The estimated accuracy of the lines is 50 kHz. The total number of measured peaks that can be attributed to formic acid was more than 40,000.

## 4. Theory

In order to analyze the infrared bands and the available rotational transitions in the seven excited vibrational states presented here, an effective rovibrational Hamiltonian in the form of a (7×7) operator matrix is required. It is formally equivalent to those used for analysis of perturbed vibrational bands of isotopically substituted modifications of formic acid molecule [16,36–39]. Rotational Hamiltonians in the diagonal blocks of this matrix determine the energies of the rovibrational levels of non-interacting vibrational states. Operators in the off-diagonal blocks are responsible for interactions between rotational levels of the corresponding vibrational states and lead to various perturbations in the spectra.

The rotational Hamiltonians in the diagonal blocks have been chosen in the form of Watson's A-reduced Hamiltonian in the $I^r$ representation

$$\begin{aligned}\langle v_i|H|v_i\rangle = {} & A\hat{J}_a^2 + B\hat{J}_b^2 + C\hat{J}_c^2 - \Delta_J\hat{J}^4 - \Delta_{JK}\hat{J}^2\hat{J}_a^2 - \Delta_K\hat{J}_a^4 \\ & + \Phi_J\hat{J}^6 + \Phi_{JK}\hat{J}^4\hat{J}_a^2 + \Phi_{KJ}\hat{J}^2\hat{J}_a^4 + \Phi_K\hat{J}_a^6 \\ & + L_J\hat{J}^8 + L_{JJJK}\hat{J}^6\hat{J}_a^2 + L_{JJKK}\hat{J}^4\hat{J}_a^4 \\ & + L_{JKKK}\hat{J}^2\hat{J}_a^6 + L_K\hat{J}_a^8 + [(-\delta_J\hat{J}^2 - \partial_K\hat{J}_a^2 \\ & + \varphi_J\hat{J}^4 + \varphi_{JK}\hat{J}^2\hat{J}_a^2 + \varphi_K\hat{J}_a^4 + I_J\hat{J}^6 \\ & + I_{JJK}\hat{J}^4\hat{J}_a^2 + I_{JKK}\hat{J}^2\hat{J}_a^4 + I_K\hat{J}_a^6), (\hat{J}_b^2 - \hat{J}_c^2)]_+ \end{aligned} \quad (1)$$

with

$$[\hat{X},\hat{Y}]_+ = \hat{X}\hat{Y} + \hat{Y}\hat{X}.$$

The axes $a$ and $b$ are in the plane of the molecule, and the $c$ axis is perpendicular to it.

The off-diagonal blocks contain rotational operators that are allowed according to the symmetry of the coupled vibrational states. They were taken in the form of sums of terms labeled with the powers of the angular momentum operators in the terms,

$$\langle v_i|H|v_j\rangle = \sum_{n,q,r} a^{\pm}_{n,q,r}\hat{h}^{\pm}_{n,q,r}, \quad (2)$$

$$\begin{aligned} \hat{h}^{\pm}_{n,q,r} &= \hat{J}^{2n}\left[\hat{J}_a^q,(\hat{J}_+^r \pm \hat{J}_-^r)\right]_+ && \text{when } r \neq 0 \text{ and } q \neq 0, \\ \hat{h}^{+}_{n,q,0} &= \hat{J}^{2n}\hat{J}_a^q && \text{when } r = 0, \\ \hat{h}^{\pm}_{n,0,r} &= \hat{J}^{2n}(\hat{J}_+^r \pm \hat{J}_-^r) && \text{when } r \neq 0 \text{ and } q = 0. \end{aligned}$$

$\hat{J}_{\pm} = \hat{J}_b \pm \hat{J}_c$ are the angular momentum ladder operators, and $a^{\pm}_{n,q,r}$ are the parameters (for the sake of simplicity, in the following sections these coefficients will also be designated as $[n, q, r, \pm]$).

Off-diagonal blocks coupling vibrational states with different symmetries contain $\hat{h}^{+}_{n,q,r}$ operators for which $q+r$ is odd, and $\hat{h}^{-}_{n,q,r}$ operators for which $q+r$ is even. If coupled vibrational states have the same symmetry then $q+r$ is even for $\hat{h}^{+}_{n,q,r}$ and odd for $\hat{h}^{-}_{n,q,r}$. Because of the phase arbitrariness of the basis functions, the vibrational basis functions of $A'$ symmetry used for construction of the total effective Hamiltonian were assumed to be real, and those of $A''$ symmetry to be imaginary. In this case the parameters $a^{\pm}_{n,q,r}$ are all real, in analogy to Ref. [24]. The phase convention for the symmetric rotor basis functions was chosen in such a way that matrix elements of the $\hat{h}^{\pm}_{n,q,r}$ operators have the form

$$\begin{aligned}\langle J,K|\hat{h}^{\pm}_{n,q,r}|J,K \pm r\rangle & \\ = J^n(J+1)^n[K^q + (K \pm r)^q] & \\ \times \prod_i^{r-1}[J(J+1) - (K \pm i)(K \pm i + 1)]^{1/2} & \end{aligned} \quad (3)$$

In Table 5 the subscripts $n$, $q$, $r$ and superscript $\pm$ are used for designation of the coupling parameters.

It should be noted that the effective Hamiltonian used in the present study is not reduced. Therefore, there is a probability of high correlation between fitted parameters. Unlike the case of an isolated vibrational state where the reduced effective rotational Hamiltonian is the same for any kind of asymmetric rotor molecule, the problem of the reduction of the effective rotational Hamiltonian for interacting vibrational states has not been considered in a general way and must be solved separately for each case. It has been previously considered only for the case of no more than two interacting states [51,52]. In the present work we did not address the problem of reducing the effective Hamiltonian because of its complexity, and used a general form given by expressions (1) and (2).

## 5. Assignment

The assignment was initiated with the identification of transitions in the $\nu_5$ band. First the relevant region of Fig. 1 had to be securely identified. The clearly distinguishable band centered at 1307 $cm^{-1}$ is not a fundamental band, though it is quite strong. It was suggested by Bertie and Michaelian [40] to be the $2\nu_9$ overtone band. In an earlier comprehensive study by Redington [8], this band was not assigned, though the $2\nu_9$ band was identified in the spectra of HCOOD, DCOOD and their $^{13}C$ and $^{18}O$ isotopic species. The anomalously high intensity for the 1307 $cm^{-1}$ band of HCOOH, as well as for $2\nu_9$ in the other isotopic modifications, is explained by a strong Fermi resonance between the $5^1$ and $9^2$ vibrational states. The assumption that the band at 1307 $cm^{-1}$ is actually $2\nu_9$ seems to be entirely sound if one looks at the observed shifts of the position of the $2\nu_9$ band expected from the harmonic

Table 6
Origins of the $\nu_5$ and $2\nu_9$ bands observed at low resolution (from Refs. [5,8])

| Band ($cm^{-1}$) | HCOOH | HCOOD | $H^{13}COOD$ | DCOOD |
|---|---|---|---|---|
| $\nu_5$ | 1223.0 | 1177.7 | 1151.0 | 1040.0 |
| $2\nu_9$ | 1307.0[a] | 1010.8 | 1007.1 | 962.8 |
| $\nu_9$ | 641.8 | 507.5 | 504.9 | 491 |
| $\nu_5$–$2\nu_9$ | −84.0 | 166.9 | 143.9 | 77.2 |
| $2\nu_9$–$2\times\nu_9$ | 23.4 | −4.2 | −2.7 | −19.2 |

[a] Observed but not assigned in [5,8].

approximation in Table 6. The band assignment was confirmed in the present study, in particular during our analysis of the $9^2 \leftarrow 9^1$ hot band. The $\nu_5$ band can then be safely assigned as the band centered at 1223 $cm^{-1}$.

At the beginning of this study we readily assigned about one thousand low $K_a$ transitions in the infrared spectrum to the $\nu_5$ and $2\nu_9$ bands. Both bands are of hybrid a- and b-type, but the $2\nu_9$ band has a more prominent central a-type Q-branch region. Since the ground state parameters were well known [4], the assignment was carried out without difficulty by the method of combination differences. Easily distinguishable, effectively unperturbed a-type ${}^{Q}Q_{K_a}$ subbranches of both bands, such as those shown in Figs. 5 and 6 for low $J$, were taken as reference transitions. These and complementary a-type transitions with $\Delta J = \pm 1$ and $\Delta K_a = 0$ and b-type transitions with $\Delta J = \pm 1$ and $\Delta K_a = \pm 1$ were used in a fit employing a model for four interacting states: $5^1$, $9^2$, $7^1 9^1$ and $7^2$. The two latter vibrational states had to be taken initially as dark states, as no data were available for these states. The four unperturbed band origins, the rotational parameters of the $5^1$ and $9^2$ states, and the principal interaction parameters were permitted to change. Initial values of the rotational parameters of the $9^2$, $7^1 9^1$ and $7^2$ states were extrapolated from the ground, $9^1$, and $7^1$ state constants [4,22]. Assumed unperturbed band origins of the $\nu_7 + \nu_9$ and $2\nu_7$ dark bands were estimated to be somewhat less than the sums determined from the $\nu_7$ and $\nu_9$ band origins. Preliminary values for the interaction parameters, which depend on Coriolis coupling parameters between the $7^1 9^1$ and $7^2$ as well as the $7^1 9^1$ and $9^2$ states, were calculated from

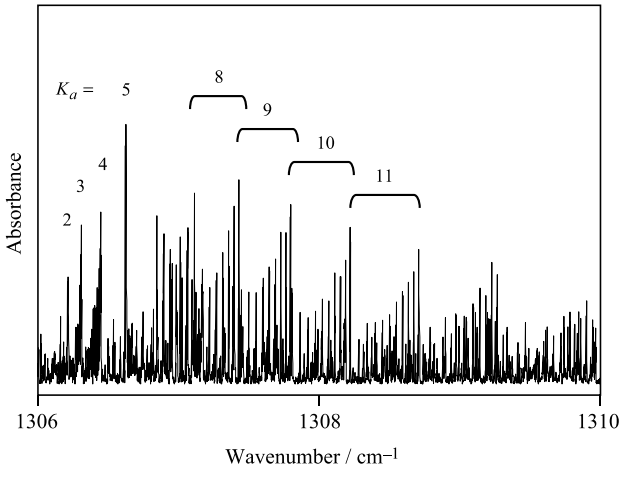


Fig. 5. Relatively unperturbed ${}^{Q}Q_{K_a}$ subbranches in the $2\nu_9$ overtone band of HCOOH.

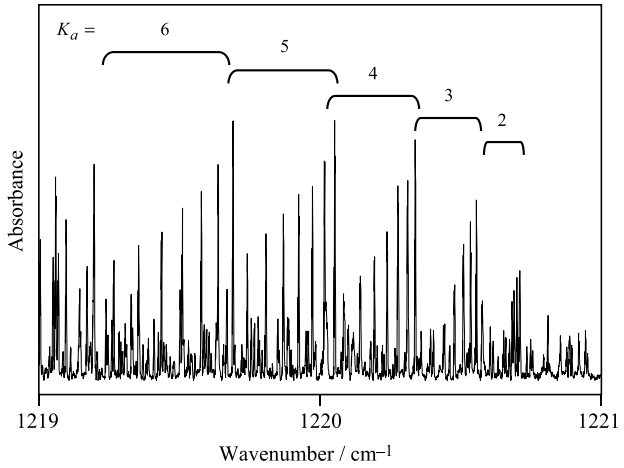


Fig. 6. Relatively unperturbed ${}^{Q}Q_{K_a}$ subbranches in the $\nu_5$ band of HCOOH.

the known parameters of the interaction between the $9^1$ and $7^1$ states [22] multiplied by $\sqrt{2}$.

From the expression for the main Coriolis coupling term in the rovibrational Hamiltonian [53], we have

$$H_{\mathrm{cor}} = -2 \sum_{\delta} A_\delta \hat{J}_\delta \pi_\delta, \tag{4}$$

where $A_\delta$ is the equilibrium rotational constant with respect to the $\delta$ principal axis of the molecule, $\pi_\delta$ is the corresponding component of the vibrational angular momentum which is

$$\pi_\delta = \sum_{kl} \left( \frac{\omega_l}{\omega_k} \right)^{1/2} \zeta_{kl}^{\delta} q_k p_l, \tag{5}$$

where $\zeta_{kl}^{\delta}$ is a Coriolis constant, $q_k$ and $p_k$ are the dimensionless $k$th normal coordinate and its conjugate momentum, and $\omega_k$ is the respective harmonic vibrational wavenumber.

From expressions (4) and (5) it follows that the main contribution to the Coriolis coupling parameter in the off-diagonal block (2) of the effective Hamiltonian between the

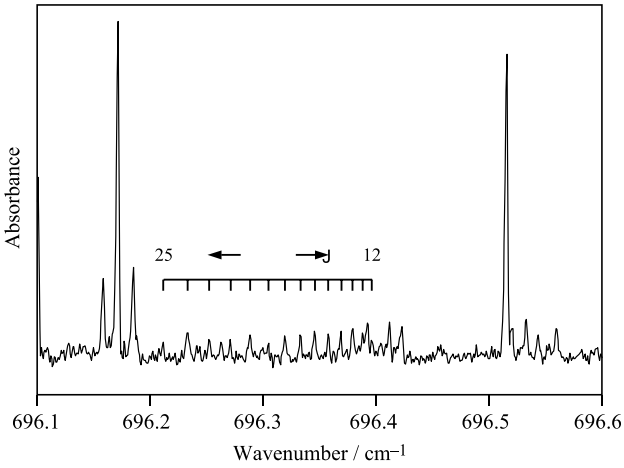


Fig. 7. The ${}^{R}Q_7$ subbranch of the hot band $9^2 \leftarrow 9^1$ of HCOOH.

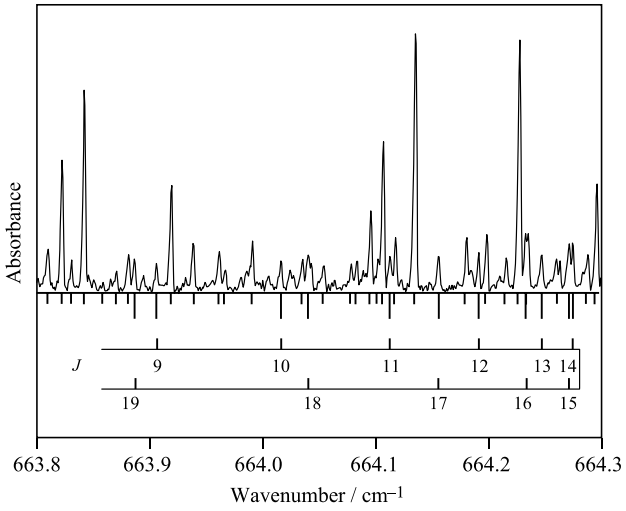


Fig. 8. The hot band $^{P}Q_1$ series, $J_{0,J}(9^2) \leftarrow J_{1,J}(9^1)$ is indicated by the long markers below the observed spectrum, while the short ticks below the spectrum mark all other assigned lines.

states $|v_7, v_9\rangle$ and $|v_7-1, v_9+1\rangle$ is

$$\langle v_7, v_9|(-1)A_\delta \pi_\delta|v_7-1, v_9+1\rangle$$

$$= -A_\delta \zeta^\delta_{79}\left[\left(\frac{\omega_7}{\omega_9}\right)^{1/2} + \left(\frac{\omega_9}{\omega_7}\right)^{1/2}\right][v_7(v_9+1)]^{1/2}. \quad (6)$$

Since in the present study the vibrational functions of $A'$ symmetry were taken to be real, and functions of $A''$ symmetry imaginary, there is a relation

$$\langle v_7 = 2, v_9 = 0|A_\delta \pi_\delta|v_7 = 1, v_9 = 1\rangle$$

$$= -\langle v_7 = 0, v_9 = 2|A_\delta \pi_\delta|v_7 = 1, v_9 = 1\rangle, \quad (7)$$

and, consequently, the Coriolis interactions coupling the $7^19^1/7^2$ and $7^19^1/9^2$ pairs of states have opposite signs.

The quartic centrifugal distortion parameters were fixed to the ground state values for all four states. The Fermi coupling constant between the $5^1$ and $9^2$ states was evaluated roughly from the data in Table 6, giving an initial value of 30 $cm^{-1}$.

The parameters of the $\nu_5$ and $2\nu_9$ bands were improved iteratively by identifying some of the observed local perturbations and including the corresponding data points into the fit. When all possible transitions to the $5^1$ and $9^2$ states identified in this manner had been included, it became necessary to find transitions to the $7^2$ and $7^19^1$ levels to expand the four-level analysis. However, it was problematic at that point. The first difficulty was the lack of precision in predicting their wavenumbers but, what was more important, it was not possible to estimate their intensity in advance and, therefore, it was not possible to be confident that they could be discerned from the noise, especially since these bands are hidden under the $\nu_5$ fundamental. Therefore, in order to obtain upper state energies for these bands, it was decided to search for the hot bands $7^2 \leftarrow 7^1$, $7^19^1 \leftarrow 7^1$ and $7^19^1 \leftarrow 9^1$ as well as $9^2 \leftarrow 9^1$ in the region of the $\nu_7$ and $\nu_9$ fundamentals. The intensities of the hot bands at room temperature should be roughly one tenth that of

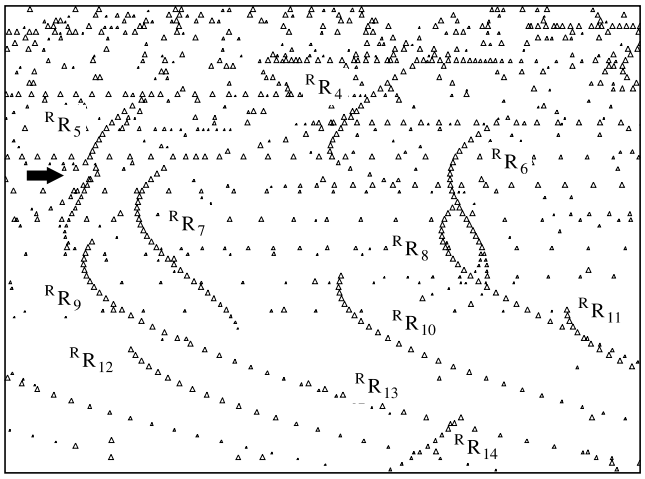


Fig. 9. Loomis–Wood diagram for the $\nu_4$ band of HCOOH with a fixed width for each row. Triangles mark line positions, with the size proportional to intensity. Each row represents a spectral segment of 0.772 $cm^{-1}$, with the upper left-hand corner corresponding to 1395 $cm^{-1}$ and the lower right-hand corner falling at about 1458 $cm^{-1}$. An intensity limit suppresses markers for weak lines for clarity. An arrow marks the perturbation of the $^{R}R_5$ subbranch caused by crossing of the $K_a=6$ levels of the $4^1$ state with the $K_a=9$ levels of the $7^19^1$ state. $^{R}R_{14}$ also appears to be strongly perturbed. There is a strong interaction of nearby levels with $K_a=15$ and $K_a=16$ of the $4^1$ and $9^2$ states, respectively.

the transitions in the $\nu_7$ and $\nu_9$ fundamentals, and that would be sufficient for their detection. Furthermore, the rotational energies of the lower states of the hot transitions are known with relatively high accuracy [22].

We thus searched for the hot bands to the dark states in the Giessen FTIR spectrum of the 430–725 $cm^{-1}$ region. Since the energies of many unperturbed rotational levels of the $9^2$ state had been determined from transitions already identified in the $2\nu_9$ band, the transitions in the $9^2 \leftarrow 9^1$ band were found

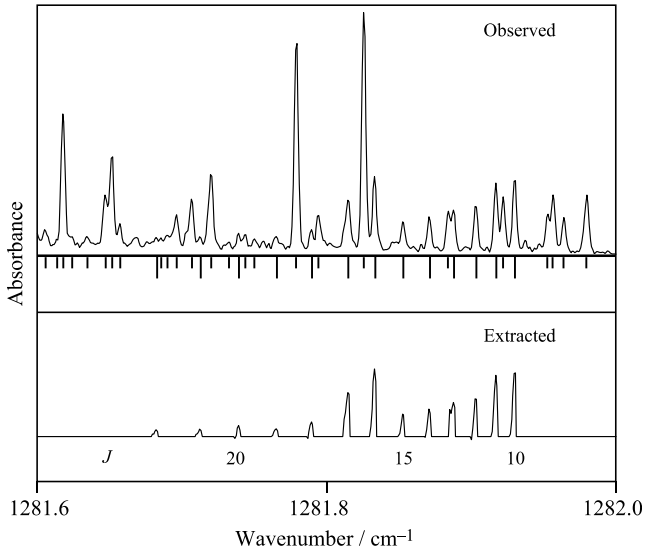


Fig. 10. The $^{Q}Q_{10}$ subbranch of the $\nu_7+\nu_9$ band. Transitions with $J=16$ and 17 are blended with $32_{2,31} \leftarrow 33_{1,32}$ and $11_{3,8} \leftarrow 12_{4,9}$ of the $2\nu_9$ band. The lower (extracted) trace, here and in further figures, shows the observed data points only for the selected series of transitions, after subtraction of all other assigned lines.

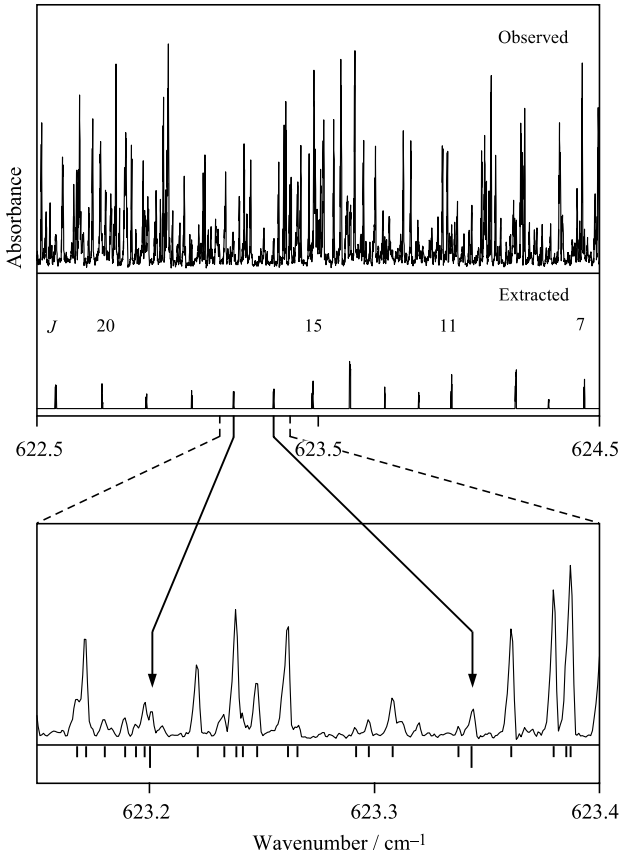


Fig. 11. Assigned series $J_{6,J-6} \leftarrow J_{5,J-4}$ in the hot band $7^1 9^1 \leftarrow 7^1$. Lower trace shows typical intensities of the hot transitions.

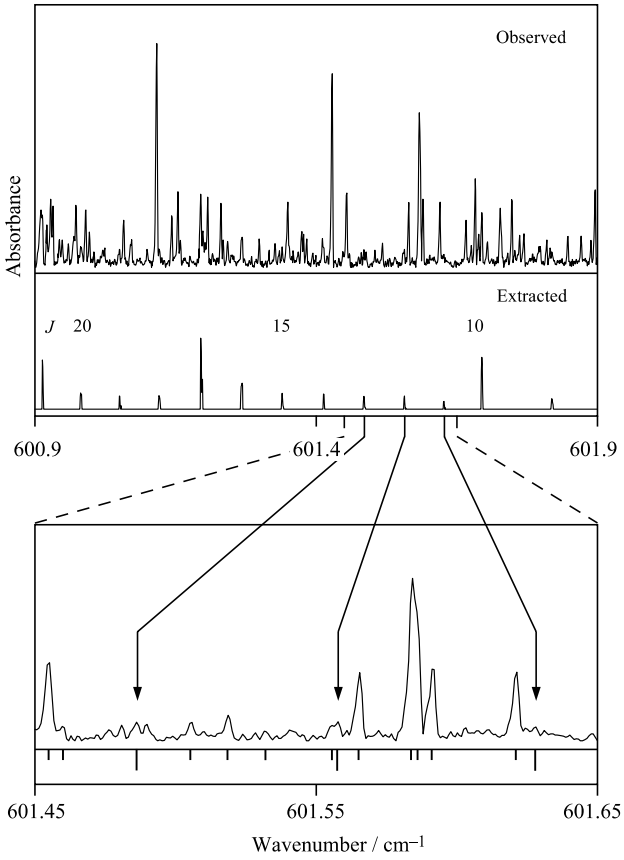


Fig. 12. Assigned series $J_{7,J-7} \leftarrow J_{6,J-6}$ in the hot band $7^1 9^1 \leftarrow 9^1$. Transitions $21_{7,14}$ ($7^1 9^1$) $\leftarrow 21_{6,15}$ ($9^1$), $17_{7,10}$ ($7^1 9^1$) $\leftarrow 17_{6,11}$ ($9^1$), $10_{7,3}$ ($7^1 9^1$) $\leftarrow 10_{6,4}$ ($9^1$) are blended with $25_{11,14} \leftarrow 26_{11,15}$, $33_{0,33} \leftarrow 34_{1,34}$, $26_{9,17} \leftarrow 27_{9,18}$ of the $\nu_7$ band. Lower trace shows typical intensities of the hot transitions.

first. In Figs. 7 and 8 the ${}^R Q_{K_a=7}$ and ${}^P Q_{K_a=1}$ branches of the $9^2 \leftarrow 9^1$ hot band are shown. The ${}^R Q_{K_a=7}$ branch is clearly distinguishable between the intense lines of the fundamental bands, which is a rare case for hot transitions. The ${}^P Q_{K_a=1}$ branch has the more characteristic appearance of such transitions, scattered among other spectral lines of various intensities. In Fig. 8, as in the following similar figures, all identified lines are indicated in order to illustrate the completeness of the assignment carried out in the present study.

The lines in the $7^2 \leftarrow 7^1$ band were assigned next, on the basis of the assumption that the $7^2$ state was less perturbed than the $7^1 9^1$ state. These and the other hot band transitions were found using a program specially designed for searching for regular series of lines in a dense spectrum. As follows from the energy level diagram (Figs. 3 and 4), the levels with medium and high $K_a$ values are not subject to local perturbations. Therefore, transitions with the same $K_a$ value and consecutive $J$ values should form regular series. After the first hot transitions in the $7^2 \leftarrow 7^1$ band had been assigned and some of the parameters of the Hamiltonian were refined, it was not difficult to find the $2\nu_7$ overtone transitions.

The constants available at this stage did not suffice to locate transitions to the last remaining dark state, $7^1 9^1$. However, at this time several hundred millimeter wave transitions belonging to the $5^1$, $9^2$ and $7^2$ vibrational states were assigned and incorporated into the fit. Furthermore, the assignment of the $\nu_4$ band was undertaken, as mentioned in Section 2.

The $\nu_4$ band is mainly of b-type, without a noticeable $Q$-branch. Identification of transitions in this band was carried out by the combination difference method and using the characteristic patterns of the ${}^R R_{K_a}$ subbranches in a Loomis–Wood diagram, as illustrated in Fig. 9. We found that the difficulty in assigning transitions to the $7^1 9^1$ state had been that it has a strong Coriolis coupling with the $4^1$ state. When the parameters including this Coriolis coupling had been refined, we eventually succeeded in assigning transitions in the $\nu_7 + \nu_9$ band. One of the $Q$-branches assigned in the $\nu_7 + \nu_9$ band is shown in Fig. 10. When the fit was enriched with these transitions of the $\nu_7 + \nu_9$ band we were able to confirm the assignments by finding transitions of both the $7^1 9^1 \leftarrow 7^1$ and $7^1 9^1 \leftarrow 9^1$ hot bands, and also millimeter wave transitions in the $7^1 9^1$ state. Transitions belonging to each of these hot bands are presented in Figs. 11 and 12, which show that the intensity of the transitions approaches the noise level.

Transitions near level crossings were added to the fit gradually, starting far from the crossing points, and as the parameters were improved, transitions closer to the crossings could be used. Otherwise, there was a risk that inaccurate parameters could calculate rotational levels that would be in

the wrong sequence, and this could bring the fit into a local minimum.

In a final stage, stimulated by remaining trends in the residuals, we added all known transitions from [16] and new FTIR and millimeter wave transitions, measured and assigned in the present work to two more vibrational states, $6^1$ and $8^1$, to the fit. Taking into account interactions with these states allowed a fine tuning of the parameters, especially those affecting rotational levels with high $K_a$. This applies not only to the five vibrational states $5^1$, $7^2$, $7^19^1$, $9^2$, and $4^1$, but also to the $6^1$ and $8^1$ states themselves. It was possible to assign and to fit IR transitions in the $\nu_6$ and $\nu_8$ bands with considerably higher $K_a$ than those included in [16].

## 6. Analysis

The spectroscopic properties of the unperturbed vibrational states are defined by the rotational and centrifugal distortion parameters of the seven considered vibrational states, while the interactions between them can be represented by the types and parameters of interaction operators necessary to reproduce the observed perturbations. In the observed spectra, interactions lead to shifts of individual subbranches, anomalies in the periodicity and intensities of otherwise regular series of transitions, and the appearance of resonance-allowed transitions. These perturbations are well described by the set of terms of the Hamiltonian and their parameters identified in the present analysis. In this section, after a presentation of the labeling scheme employed, some examples of the effects of the perturbations in various regions of the spectra and explanations on the basis of the observed energy level diagram (Figs. 3 and 4) and the set of parameters obtained in the analysis (Tables 4 and 5) are given.

### 6.1. State and eigenfunction labeling scheme

Labeling of the energies for severely mixed states is not straightforward since the vibrational quantum numbers $v$ and asymmetric rotor pseudo-quantum numbers $K_a$ and $K_c$ are not conserved in such a situation; the only good quantum number is $J$. However, in the present study a labeling scheme consistent with conventional labeling was used. Each eigenstate $|\Psi_i\rangle$ is marked by the vibrational and rotational quantum numbers which correspond to one of the basis functions in the expansion of the overall wavefunction of the mixed state

$$|\Psi_i\rangle = \sum_{v',K_a'} C^{(i)}_{v',J,K_a',K_c'} |v',J,K_a',K_c'\rangle, \tag{8}$$

where $C^{(i)}_{v',J,K_a',K_c'}$ is a coefficient of a basis function $|v',J,K_a',K_c'\rangle$. Here $|v',J,K_a',K_c'\rangle$ is a product of the many-dimensional harmonic vibrational wavefunction $|v'\rangle$ and the semirigid (effective) asymmetric top wavefunction $|J,K_a',K_c'\rangle$. The wavefunction $|v'\rangle$ corresponds to one of the seven vibrational states under consideration and the wavefunction $|J,K_a',K_c'\rangle$ is an eigenfunction in the vibrational state $|v'\rangle$. $K_c$ is unambiguously determined by the symmetry of the level and by $J$ and $K_a$.

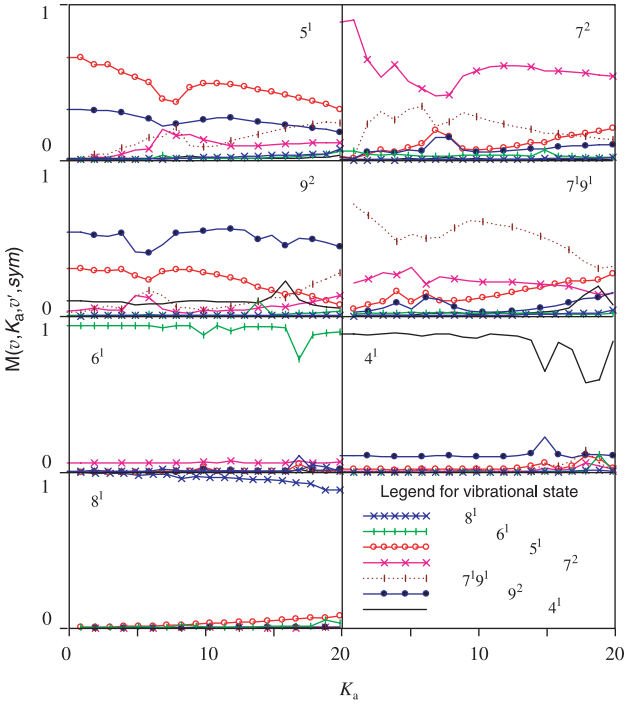


Fig. 13. The dependence of the mixing coefficients $M(v,K_a,v',\mathrm{sym})$ on $v'$ and $K_a$ for levels of symmetry $A'$. The vibrational state $v$ is indicated on each plot.

One choice of labels would be to take the quantum numbers of the largest coefficient $C^{(i)}_{v',J,K_a',K_c'}$, but in a few instances of strong interactions this labeling would fail because it does not truly reflect the vibrational state. The method used in the present analysis was to calculate the sum of the squared coefficients over $K_a'$ for each value of $v'$ and $J$:

$$\sum_{K_a'} \left| C^{(i)}_{v',J,K_a',K_c'} \right|^2. \tag{9}$$

The sum gives the probability with which the level $|\Psi_i\rangle$ for a given $J$ belongs to the vibrational state $|v'\rangle$. Then the largest $|C^{(i)}_{v',J,K_a',K_c'}|^2$ of all the terms in the largest of these sums (9) is taken to define the quantum numbers for the rovibrational level described by $|\Psi_i\rangle$. However, even this way of level labeling is not ideal and like others has shortcomings: in the presence of several interacting states, situations can arise where more than one level may have the same identification. Therefore in the supplementary tables, the indices of the eigenvalues assigned by the program are employed as an unambiguous auxiliary label.

After the identifying rovibrational level has been selected as discussed above, it is then convenient to mark wavefunctions $|\Psi_i\rangle$ as $|\Psi_{v,J,K_a,K_c}\rangle$ and expansion coefficients as $C^{(v,K_a,K_c)}_{v',J,K_a',K_c'}$, where superscripts determine the eigenstate and subscripts show the quantum numbers of the basis function in (8). $J$ is the same for the state and basis functions, so it is shown only among subscripts.

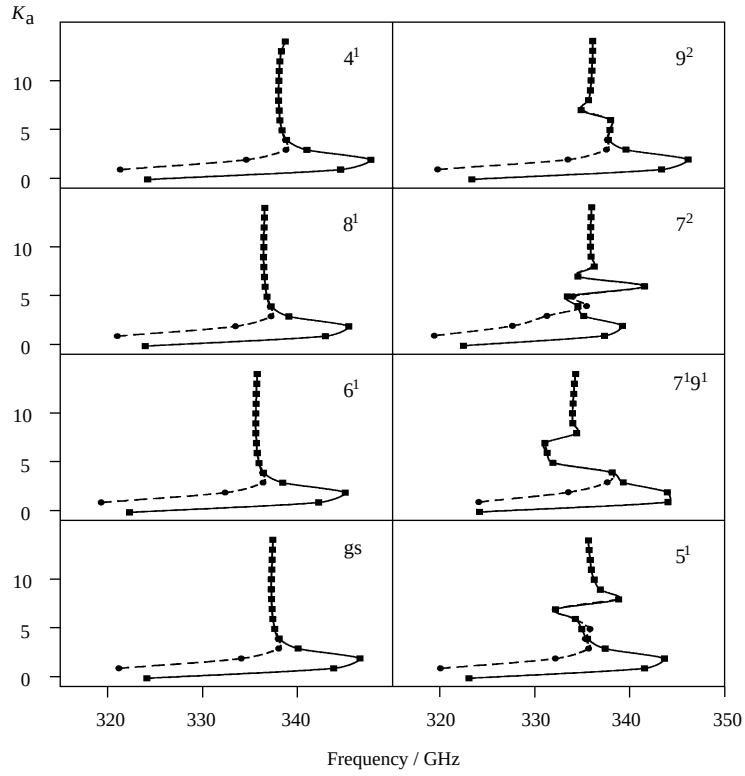


Fig. 14. Fortrat diagrams of $J=14$ a-type rotational transitions plotted versus $K_a$ for eight vibrational states of HCOOH.

### 6.2. Global interactions

First of all, we will consider *the global interactions* among the vibrational states caused by Fermi interactions and a-, b- and c-type Coriolis interactions. These lead to shifts of large manifolds of rotational and rovibrational transitions. A Fermi interaction (selection rule $\Delta K_a=0$) is, to first order, homogeneous, i.e. it depends only on a difference between the vibrational quantum numbers. An a-type Coriolis interaction ($\Delta K_a=0$) increases with $K_a$ while b- and c-type interactions ($\Delta K_a=\pm 1$) go up with $J$. Although all seven investigated vibrational states interact with each other, the degrees of the various perturbations differ widely. A qualitative measure of the extent of mixing of states in the case of such global interactions can be given in terms of a reduced mixing coefficient, which we define as

$$M(v,K_a,v',\mathrm{sym}) = \sum_{J',K_a'} |C^{(v,K_a,K_c)}_{v',J,K_a',K_c'}|^2/n. \qquad (10)$$

Here, sym denotes the symmetry of the rovibrational level, $A'$ or $A''$, and $v'$ is fixed successively to each of the vibrational states involved; $n$ is the number of terms in the sum. In our case the range of $J'$ is roughly 0–50. The resulting values of $M(v, K_a, v', \mathrm{sym})$ represent the mixing, averaged over $J$, of the different vibrational states $v'$ in the rovibrational levels with given $v$, $K_a$. Fig. 13 presents the dependence of $M(v, K_a, v', \mathrm{sym})$ on $v'$ and $K_a$ in the case of sym$=A'$. The corresponding graphs for $A''$ symmetry are practically the same. The global perturbations indicated in Fig. 13 are seen when the curves in the energy level diagrams of Figs. 3 and 4 are close and parallel. The uppermost curve in each figure corresponds to the $M(v, K_a, v', \mathrm{sym})$ for which $v=v'$. By definition, the sum of all the curves gives a straight line at unit level, i.e. $\sum_{v'} M(v,K_a,v',\mathrm{sym}) = 1$. From the graphs in Fig. 13 it can be deduced that the $8^1$, $6^1$ and $4^1$ states are the least perturbed, while the $5^1$, $9^2$, $7^2$ and $7^19^1$ states interact strongly. These latter states interact mainly according to the primary scheme involving $5^1/9^2$ (Fermi interaction, with an interaction parameter of 42 cm$^{-1}$ and a difference of the unperturbed vibrational state origins of 40 cm$^{-1}$, Table 5), $9^2/7^19^1$, and $7^2/7^19^1$ (both of these dyads having a- and b-type Coriolis interactions, with interaction parameters of 1.6 and 0.24 cm$^{-1}$ for the $7^2/7^19^1$ dyad and 1.2 and 0.15 cm$^{-1}$ for the $9^2/7^19^1$ states and an unperturbed energy difference of the band centers in both cases of about 20 cm$^{-1}$). As a result of this primary scheme, secondary effects involving all the states occur. For example, due to the considerable Fermi interaction $9^2/5^1$ there are rather strong contributions of the $7^19^1$ and $7^2$ states to $5^1$ via the $9^2$ state. At the same time there is of course an opposite effect, i.e. each of the states $9^2$, $7^2$ and $7^19^1$ has a significant component from the three others, including $5^1$. It should be noted that due to the very strong Fermi resonance between $5^1$ and $9^2$ and to its homogenous nature, the relative extent of mixing of these states depends only weakly on the rotational quantum numbers. Therefore, the ratio of the coefficients

$$\frac{\sum_{K_a'} \left| C^{(v,K_a,K_c)}_{5^1,J,K_a',K_c'} \right|^2}{\sum_{K'} \left| C^{(v,K_a,K_c)}_{9^2,J,K_a',K_c'} \right|^2}$$

for all rotational levels in the $v=5^1$ state is about 2, while in the $v=9^2$ state it is about 0.5.

Irregularities of the curves in Fig. 13 with $K_a$ are explained by the unequal arrangement of the strongly interacting energy levels for certain values of $K_a$ for the different vibrational states. For instance, the pronounced dip in the uppermost curve in Fig. 13 for the $5^1$ state can be explained by the proximity of the $K_a=7$ levels of $5^1$ to the $K_a=5$ levels of $7^19^1$, and similarly the proximity of the $5^1$ levels with $K_a=8$ to the $7^19^1$ and $7^2$ levels with $K_a=6$ and 7, respectively (Fig. 3). Indeed, for the strongly interacting states $5^1$, $9^2$, $7^2$ and $7^19^1$ the largest and most irregular interactions occur for $K_a$ in the region 5–8, which is due to a crowding of levels which can interact.

The energy levels of the $7^19^1$ and $7^2$ states show an especially peculiar behavior. The level series of these states for which $\Delta K_a=1$ are separated by only small energy intervals over a long range of $J$, so that they lie almost parallel with each other. This is an ideal condition for the appearance of a global b-type Coriolis interaction, and is responsible for the form of the relevant curves in Figs. 13, 3 and 4.

The magnitude of the perturbations of different vibrational states is clearly observed in the rotational spectra of these states. Since, the permanent electric dipole moment component $\mu_a=1.42$ D is much larger than $\mu_b=0.26$ D [25], a-type transitions dominate in the pure rotational spectrum and the strongest and most characteristic are the ${}^aR(J)_{0,1}$ branches with $\Delta K_a=0$ and $\Delta K_c=1$. For each $J$ the various $K_a$ transitions of these branches form a cluster with a typical structure [54]. The separation between clusters with adjacent $J$ values is roughly $(B+C)=0.75\ \mathrm{cm}^{-1}$. For high $K_a$ (close to $J$) the lines form a compact group or bandhead, and each line is degenerate in $K_c$. The asymmetry splitting of transitions with low $K_a$ diverges with $J$ to opposite sides of the kernel of each cluster and may overlap the region of the next cluster for $K_a=1$. Fig. 14 illustrates the degree of perturbation of the ${}^aR(14)_{0,1}$ clusters for all eight vibrational states treated in this study. It can be readily seen that rotational transitions are almost unperturbed in the $8^1$, $4^1$, and $6^1$ states, since their clusters have the same appearance as for the ground state. On the contrary, the rotational transitions are significantly disturbed in the $5^1$, $9^2$, $7^2$, and $7^19^1$ states, in correspondence with the above considerations.

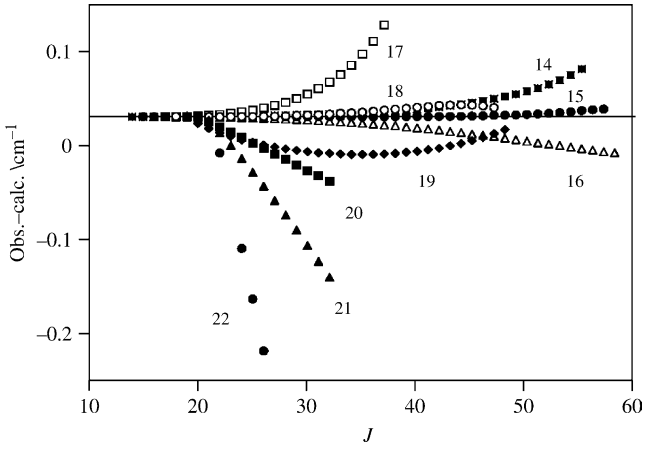


Fig. 15. Residuals obtained when the parameters of Ref. [16] are used to predict the energies of the rotational levels of the $6^1$ state of HCOOH. Each curve (only those for $K_a>13$ are shown) is labeled with the value of $K_a$.

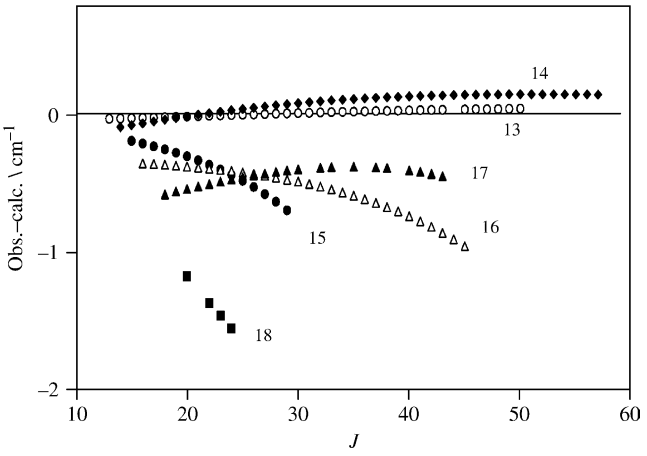


Fig. 16. Residuals obtained for the energies of the rotational levels of the $4^1$ state of HCOOH when no interactions with this state are fitted. Each curve (only those for $K_a>12$ are shown) is labeled with the value of $K_a$.

The effect of the global perturbations, especially the $J$- and $K_a$-dependent Coriolis perturbations, in the form of the displacement of energy level series as a function of $K_a$, is illustrated in Figs. 15 and 16. Fig. 15 presents the differences between observed term values of the $6^1$ state and calculated values obtained using parameters from [16]. (The observed values were averaged over all transitions having the same upper level.) Only transitions with $K_a>13$ are shown, since the perturbation is weaker at low $K_a$. In Ref. [16] only the interactions between the $6^1$ and $8^1$ states were taken into account. From Fig. 15 it can be seen that the residual discrepancies due to other interactions reach more than $0.2\ \mathrm{cm}^{-1}$. In Table 7 we compare the maximal quantum number $J$ of the transitions assigned and fitted for the indicated values of $K_a$ in the present work and in [16]. For $K_a$ less than 10, the maximal values of $J$ are about the same, while for higher $K_a$ the effect of including other vibrational states in the fit allows the fit to be extended significantly. In Ref. [16] only

Table 7
Comparison of the maximal $J$ for different $K_a$for the transitions in the $\nu_6$ band assigned and fitted in the present work and in Ref. [16]

| | $J_{max}$ | | | $J_{max}$ | |
|---|---|---|---|---|---|
| $K_a$ | Ref. [16] | Present work | $K_a$ | Ref. [16] | Present work |
| 0 | 67 | 75 | 12 | 42 | 59 |
| 1 | 68 | 76 | 13 | 29 | 57 |
| 2 | 70 | 76 | 14 | 24 | 52 |
| 3 | 63 | 70 | 15 | 40 | 57 |
| 4 | 65 | 65 | 16 | 23 | 57 |
| 5 | 53 | 62 | 17 | 19 | 35 |
| 6 | 58 | 71 | 18 | 27 | 47 |
| 7 | 64 | 65 | 19 | | 48 |
| 8 | 58 | 58 | 20 | | 42 |
| 9 | 56 | 65 | 21 | | 34 |
| 10 | 29 | 58 | 22 | | 26 |
| 11 | 37 | 53 | | | |

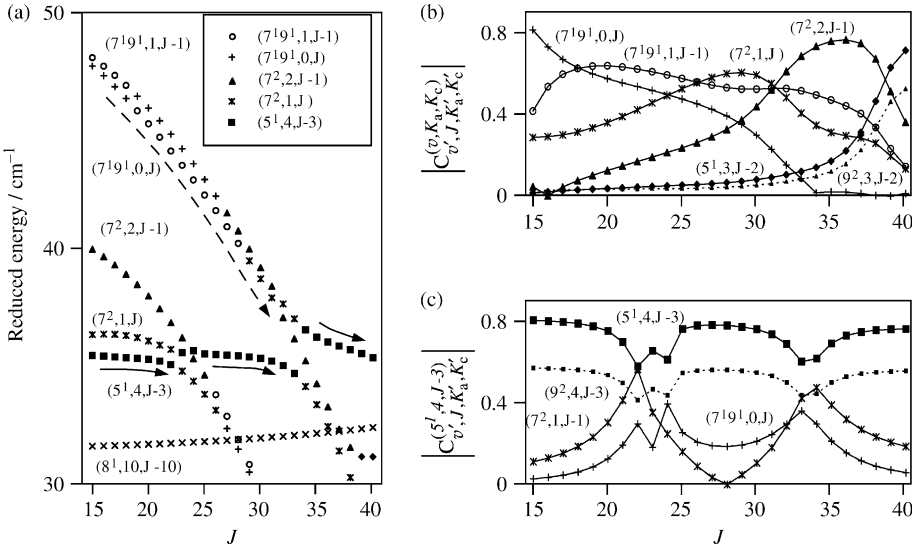


Fig. 17. Examples of local perturbations with level crossings in HCOOH: (a) reduced energy plot involving rotational levels of three vibrational states indicated in the legend; (b) and (c) coefficients of the vibrational basis functions in the eigenfunctions for the indicated states and levels, indicated by $(n^i, K_a, K_c)$, where $n$ is the normal mode and $i$ is the value of $v_n$.

those transitions were used for which the curves in Fig. 15 lie near the zero line, while in the present work all levels depicted in Fig. 15 were included in the fit.

Another example of displacement of energy levels with large $K_a$ is given in Fig.16. This figure shows the differences between observed and calculated values for levels with $K_a \geq 13$ of the $4^1$ state found using parameters obtained when this state was treated as isolated. In this case the differences reach 1.5 cm$^{-1}$ for $K_a = 18$.

### 6.3. Local perturbations

In many regions of the recorded spectra, *local perturbations* become apparent when energy levels of different vibrational states cross. The magnitude of local perturbations is large when the differences in $K_a$ are small. It is interesting to find the maximal difference in $K_a$ for which they are distinguishable under the given experimental conditions, and how well the parameters obtained in the present study reproduce the observed anomalies in the spectrum. Some typical examples of local perturbations are illustrated in Fig. 17.

In Fig. 17(a) a portion of the energy level diagram of Fig. 3, containing intersections of several energy level series of $A''$ symmetry with $K_a = 4$ of the $5^1$ vibrational state, is enlarged. Fig. 17(a) contains precise information about multiple changes of the vibrational and/or rotational state, along an apparent series of levels, which can appear in the case of several strongly interacting vibrational states. For the sake of simplicity in this discussion, the labels of the apparent energy series in Figs. 3 and 17 are taken to be those arrived at by the procedure described above for the eigenvalues with small $J$. For example, if one follows along the dashed arrow in Fig. 17(a) which follows the series marked as $(v, K_a, K_c) = (7^19^1, 0, J)$, then the levels up to $J = 18$ belong to the $|\Psi_{7^19^1,J,0,J}\rangle$ levels and then above $J = 18$ they are already $|\Psi_{7^19^1,J,1,J-1}\rangle$ levels. The next three points belong to the $|\Psi_{7^2,J,1,J}\rangle$ state and the next points become $|\Psi_{7^2,J,2,J-1}\rangle$ states. This behavior is explained by Fig. 17(b), where the dependence of the absolute values of the most significant expansion coefficients $C^{(v,K_a,K_c)}_{v',J,K_a',K_c'}$ on $J$ are shown. Those curves in Fig. 17(b) which succeed in being the highest determine the quantum numbers of the label of the level. We observe the same effect for other series, $(7^19^1, 1, J-1)$, $(7^2, 1, J)$ and $(7^2, 2, J-1)$. State changing along the series is usually observed for small $K_a$ since due to asymmetry effects, there is more chance of an intersection of strongly interacting states. For high $K_a$, the

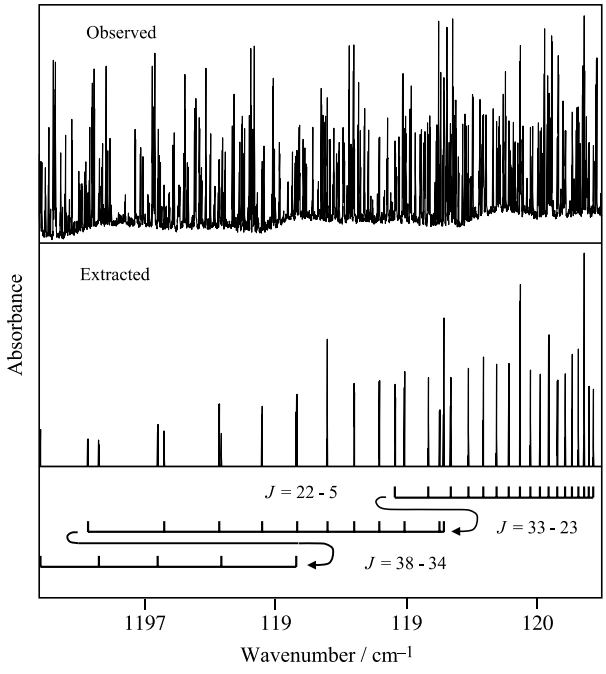


Fig. 18. Perturbations in the observed spectrum corresponding to the reduced energies shown in Fig. 17. A portion of the $^PQ_5$ subbranch of the $\nu_5$ band is shown. The wavenumbers and their residuals are given in Table 8.

Table 8
Transitions of the $^{P}Q_5$ subbranch of the $\nu_5$ band of HCOOH

| Wavenumber ($cm^{-1}$) | $J'$ | $K_a'$ | $K_c'$ | $J''$ | $K_a''$ | $K_c''$ | (O-C)×$10^3$ ($cm^{-1}$) | Relative intensity | Wavenumber ($cm^{-1}$) | $J'$ | $K_a'$ | $K_c'$ | $J''$ | $K_a''$ | $K_c''$ | (O-C)×$10^3$ ($cm^{-1}$) | Relative intensity |
|---|---|---|---|---|---|---|---|---|---|---|---|---|---|---|---|---|---|
| 1200.4349 | 5 | 4 | 2 | 5 | 5 | 1 | −0.3 | 0.18 | 1199.2929 | 23 | 4 | 20 | 23 | 5 | 19 | −0.8 | 0.29 |
| 1200.4019 | 6 | 4 | 3 | 6 | 5 | 2 | 0.5 | 0.20 | 1199.2603 | 24 | 4 | 21 | 24 | 5 | 20 | −0.4 | 0.16 |
| 1200.3644 | 7 | 4 | 4 | 7 | 5 | 3 | 0.6 | 0.53 | 1198.9914 | 25 | 4 | 22 | 25 | 5 | 21 | −0.4 | 0.24 |
| 1200.3211 | 8 | 4 | 5 | 8 | 5 | 4 | 0.6 | 0.28 | 1198.8000 | 26 | 4 | 23 | 26 | 5 | 22 | −0.2 | 0.23 |
| 1200.2731 | 9 | 4 | 6 | 9 | 5 | 5 | 1.0 | 0.28 | 1198.6080 | 27 | 4 | 24 | 27 | 5 | 23 | −0.3 | 0.20 |
| 1200.2191 | 10 | 4 | 7 | 10 | 5 | 6 | 0.4 | 0.20 | 1198.4023 | 28 | 4 | 25 | 28 | 5 | 24 | 0.4 | 0.32 |
| 1200.1601 | 11 | 4 | 8 | 11 | 5 | 7 | 0.0 | 0.22 | 1198.1708 | 29 | 4 | 26 | 29 | 5 | 25 | −0.1 | 0.17 |
| 1200.0277 | 13 | 4 | 10 | 13 | 5 | 9 | 0.1 | 0.23 | 1197.9029 | 30 | 4 | 27 | 30 | 5 | 26 | 0.1 | 0.18 |
| 1199.9537 | 14 | 4 | 11 | 14 | 5 | 10 | 0.0 | 0.23 | 1197.5771 | 31 | 4 | 28 | 31 | 5 | 27 | −0.1 | 0.18 |
| 1199.8750 | 15 | 4 | 12 | 15 | 5 | 11 | 0.9 | 0.44 | 1197.1554 | 32 | 4 | 29 | 32 | 5 | 28 | −0.1 | 0.11 |
| 1199.7885 | 16 | 4 | 13 | 16 | 5 | 12 | 0.1 | 0.25 | 1196.5727 | 33 | 4 | 30 | 33 | 5 | 29 | 0.2 | 0.10 |
| 1199.6957 | 17 | 4 | 14 | 17 | 5 | 13 | 0.0 | 0.24 | 1198.1652 | 34 | 4 | 31 | 34 | 5 | 30 | 0.6 | 0.16 |
| 1199.5941 | 18 | 4 | 15 | 18 | 5 | 14 | 0.1 | 0.21 | 1197.5924 | 35 | 4 | 32 | 35 | 5 | 31 | −0.3 | 0.10 |
| 1199.4801 | 19 | 4 | 16 | 19 | 5 | 15 | 0.0 | 0.25 | 1197.1071 | 36 | 4 | 33 | 36 | 5 | 32 | −0.5 | 0.13 |
| 1199.3463 | 20 | 4 | 17 | 20 | 5 | 16 | 0.0 | 0.23 | 1196.6560 | 37 | 4 | 34 | 37 | 5 | 33 | −0.1 | 0.08 |
| 1199.1743 | 21 | 4 | 18 | 21 | 5 | 17 | 0.0 | 0.21 | 1196.2092 | 38 | 4 | 35 | 38 | 5 | 34 | 0.5 | 0.11 |
| 1198.9200 | 22 | 4 | 19 | 22 | 5 | 18 | −0.3 | 0.21 | | | | | | | | | |

assignment of the levels along a series, as a rule, does not change. For instance, the levels with $K_a=10$ for the $8^1$ state which fall into the region of Fig. 17(a) do not feel any noticeable influence from the other levels, which have significantly smaller $K_a$, and assignments of all levels in that series do not change over the observed range of $J$.

The series labeled as $K_a=4$ levels of the $5^1$ state has discontinuities at crossing points with other branches. Intersections take place with the $K_a=1$ and 2 levels of the $7^2$ state in the region of $J=23$–24 and with the $K_a=0$ and 1 levels of the $7^19^1$ state for $J=33$–34. Naturally, corresponding perturbations appear in the observed spectra. A portion of the spectrum containing the $^{P}Q_5$ subbranch of the $\nu_5$ band is shown in Fig. 18 and the corresponding wavenumbers and their residuals are given in Table 8. In the absence of any perturbations the observed subbranch $^{P}Q_5$ should be a regular series with monotonically decreasing frequencies. In reality there are 'faults' corresponding in $J$ to the points of crossings with other energy level series. At the same time it should be noted that despite significant perturbations, reaching 1.5 $cm^{-1}$, the parameters determined for the Hamiltonian describe the observed perturbations well.

The interaction of singly excited states with combination and overtone states leads to well-known effects in the spectrum, in particular substantial increases in the intensities of some overtone and combination branches or subbranches and the appearance of resonance-allowed transitions.

Fig. 17(c) shows the behavior of the $|\Psi_{5^1,J,4,J-3}\rangle$ eigenfunctions with $J$. In the regions of strong interaction there is significant admixing of other components, especially of $|7^2,J,1,J\rangle$. In turn, because of the reciprocity of the interactions, there are contributions from the $|5^1,J,4,J-3\rangle$ basis function to the $|\Psi_{7^2,J,1,J}\rangle$ eigenstates and the intensity of IR transitions to the $(7^2,1,J)$ levels should be increased. Indeed, we were able

Table 9
Perturbation-enhanced transitions in the $2\nu_7$ band of HCOOH

| Wavenumber ($cm^{-1}$) | $J'$ | $K_a'$ | $K_c'$ | $J''$ | $K_a''$ | $K_c''$ | (O-C)×$10^3$ ($cm^{-1}$) | Relative intensity | Wavenumber ($cm^{-1}$) | $J'$ | $K_a'$ | $K_c'$ | $J''$ | $K_a''$ | $K_c''$ | (O-C)×$10^3$ ($cm^{-1}$) | Relative intensity |
|---|---|---|---|---|---|---|---|---|---|---|---|---|---|---|---|---|---|
| 1215.1664 | 20 | 1 | 19 | 19 | 5 | 14 | −0.8 | 0.02 | 1177.6320 | 25 | 1 | 24 | 26 | 5 | 21 | 0.5 | 0.05 |
| 1184.3222 | 20 | 1 | 19 | 21 | 5 | 16 | 0.3 | 0.05 | 1174.4651 | 32 | 1 | 31 | 33 | 5 | 28 | −0.1 | 0.02 |
| 1200.1263 | 20 | 1 | 19 | 20 | 5 | 16 | −0.1 | 0.04 | 1198.8861 | 33 | 1 | 32 | 33 | 5 | 29 | −0.1 | 0.08 |
| 1235.1043 | 21 | 1 | 20 | 21 | 3 | 19 | 0.0 | 0.11 | 1200.7016 | 33 | 1 | 32 | 34 | 3 | 31 | −0.1 | 0.06 |
| 1215.6494 | 21 | 1 | 20 | 20 | 5 | 15 | 0.7 | 0.01 | 1215.7339 | 33 | 1 | 32 | 33 | 4 | 29 | −0.8 | 0.02 |
| 1183.2875 | 21 | 1 | 20 | 22 | 5 | 17 | 0.1 | 0.06 | 1212.1152 | 34 | 1 | 33 | 34 | 4 | 30 | 0.0 | 0.04 |
| 1199.8524 | 21 | 1 | 20 | 21 | 5 | 17 | 0.1 | 0.06 | 1196.2876 | 34 | 1 | 33 | 35 | 3 | 32 | 0.3 | 0.07 |
| 1234.8477 | 22 | 1 | 21 | 22 | 3 | 20 | −0.1 | 0.17 | 1195.7627 | 34 | 1 | 33 | 34 | 5 | 30 | 0.4 | 0.05 |
| 1216.1125 | 22 | 1 | 21 | 21 | 5 | 16 | −0.3 | 0.02 | 1241.1651 | 34 | 1 | 33 | 33 | 4 | 30 | 0.4 | 0.14 |
| 1182.2331 | 22 | 1 | 21 | 23 | 5 | 18 | −0.5 | 0.13 | 1168.6723 | 34 | 1 | 33 | 35 | 5 | 30 | 0.2 | 0.03 |
| 1199.5607 | 22 | 1 | 21 | 22 | 5 | 18 | −0.1 | 0.13 | 1194.7270 | 35 | 1 | 34 | 35 | 5 | 31 | 0.1 | 0.04 |
| 1215.8286 | 23 | 1 | 22 | 22 | 5 | 17 | −0.8 | 0.02 | 1240.9653 | 35 | 1 | 34 | 34 | 4 | 31 | 0.5 | 0.09 |
| 1180.4304 | 23 | 1 | 22 | 24 | 5 | 19 | 0.3 | 0.05 | 1233.1009 | 35 | 1 | 34 | 35 | 3 | 33 | −0.3 | 0.03 |
| 1233.3734 | 24 | 1 | 23 | 24 | 3 | 22 | 0.0 | 0.04 | 1187.5543 | 35 | 1 | 34 | 36 | 4 | 33 | 0.3 | 0.03 |
| 1179.1034 | 24 | 1 | 23 | 25 | 5 | 20 | 0.4 | 0.03 | 1193.9937 | 35 | 1 | 34 | 36 | 3 | 33 | 0.6 | 0.02 |
| 1197.9637 | 24 | 1 | 23 | 24 | 5 | 20 | 0.2 | 0.03 | 1233.1009 | 35 | 1 | 34 | 35 | 3 | 33 | −0.3 | 0.03 |
| 1232.7676 | 25 | 1 | 24 | 25 | 3 | 23 | −0.7 | 0.04 | 1232.4351 | 36 | 1 | 35 | 36 | 3 | 34 | 0.4 | 0.04 |

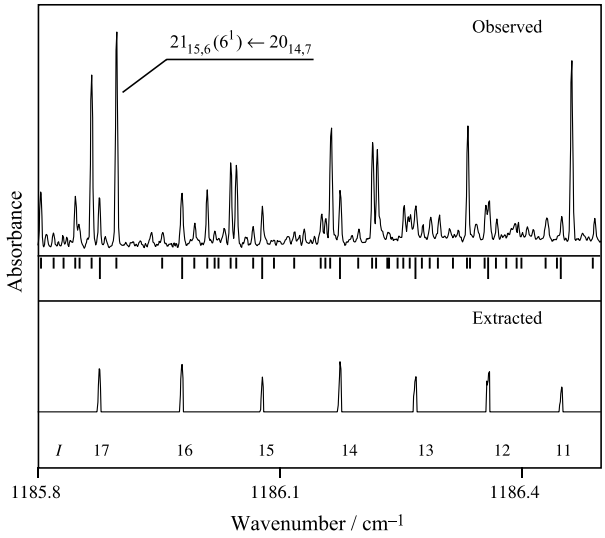


Fig. 19. Resonance-enhanced subbranch $J_{5,J-5} \leftarrow J_{8,J-8}$ of the $\nu_7+\nu_9$ band. A strong transition, $21_{15,6} \leftarrow 20_{14,7}$ of the $\nu_6$ band, is shown for a comparison of the intensities.

to assign such perturbation-enhanced transitions and use them in the fit with the results shown in Table 9.

In Fig. 13 there are several peaks on the $5^1$ state mixing curves for the $7^19^1$ and $7^2$ states. They correspond to those $K_a$ values of the $7^19^1$ and $7^2$ states where significant interactions

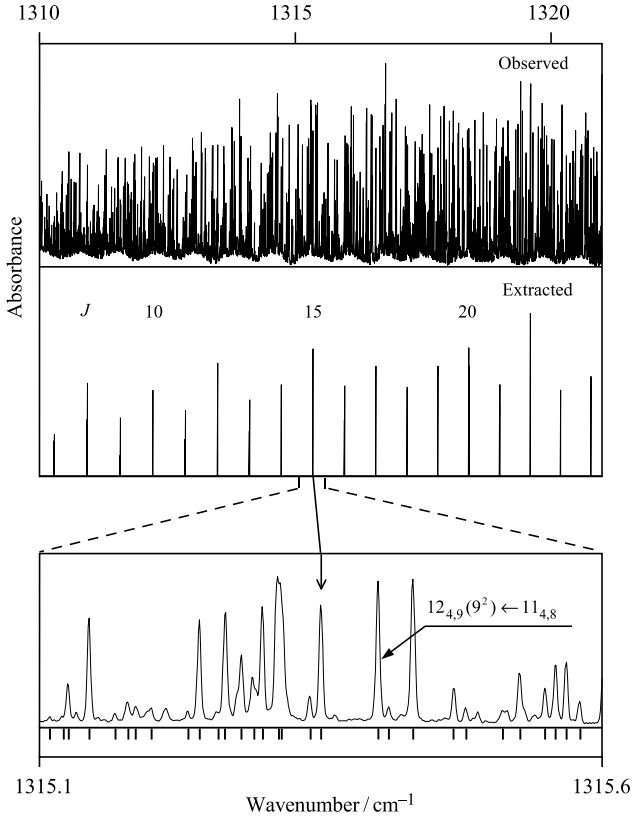


Fig. 20. The b-type $R$-branch series $J_{7,J-7}(7^19^1) \leftarrow J-1_{6,J-7}$ (gs), enhanced by perturbation. The middle trace shows transitions of the series extracted from the measured spectrum. The lower picture shows a fragment of the spectrum containing one transition of the series. The inherently strong transition $12_{4,9} \leftarrow 11_{4,8}$ of the $2\nu_9$ band is shown for a comparison of the intensities.

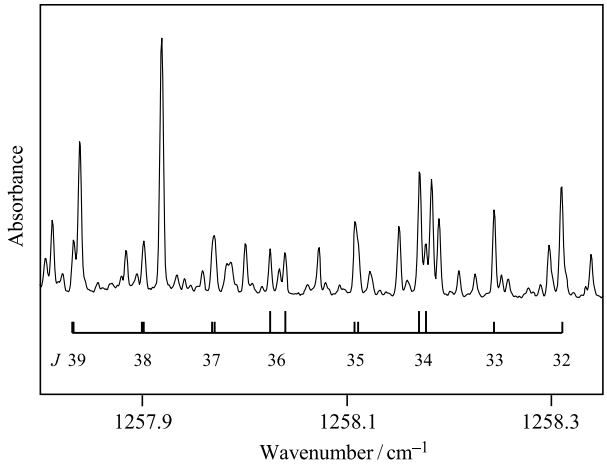


Fig. 21. Asymmetry splitting in the $^RQ_9$ subbranch of the $\nu_5$ band of HCOOH, due to the interaction of the (unsplit) $K_a=10$ levels of $v_5=1$ of different symmetry with the (asymmetry-split) $K_a=5$ levels of $v_4=1$.

with the $5^1$ state occur. These are at $K_a=4$, 5, 7 for the $7^19^1$ state and $K_a=7$ for the $7^2$ state. Detailed analysis of the wavefunctions for these $K_a$ values shows that the $K_a=4$, 5 and 7 basis functions of the $7^19^1$ vibrational state are mixed respectively with $K_a=6$, 7 and 6 of the $5^1$ state, and $K_a=7$ of the $7^2$ state interacts with $K_a=8$ of the $5^1$ state. This gives rise to transitions with selection rules $\Delta K_a=2$, 3. Fig. 19 presents an example of the resonance-allowed subbranch $J_{5,J-5} \leftarrow J_{8,J-8}$ in the $\nu_7+\nu_9$ band. It appears due to mixing of the $|7^19^1,J,K_a=5,K_c=J-5\rangle$ basis function into the $|5^1,J,K_a=7,K_c=J-6\rangle$ eigenfunction. Another example of anomalously high intensity of transitions into the $7^19^1$ state is shown in Fig. 20.

A difference in term values for $A'$ and $A''$ symmetries for the same $K_a$ values, due to asymmetry splitting, is indicated in Figs. 3 and 4 for low $K_a$ values, and this may lead to the splitting of otherwise degenerate doublets for higher $K_a$ at crossing points. Fig. 21 illustrates such a situation which was observed in the $^RQ_{K_a=9}$ subbranch of the $\nu_5$ band. The nearly degenerate $K_a=10$ levels of the $5^1$ state cross the $K_a=5$ levels of $A'$ symmetry of the $4^1$ state near $J=33$, while the same levels of $A''$ symmetry cross near 36. As a result, there are two resolved doublets, at $J=34$ and 36, which normally would not be split, each doublet containing one unshifted line. This example also demonstrates that differences in $K_a$ up to 5 between interacting states can lead to clearly detectable perturbations.

Another effect which is manifested in Fig. 17(a) is the same rovibrational identification of two different levels. The levels $J=26_{1,26}$, $27_{1,27}$ and $28_{1,28}$ of the $7^19^1$ state (unfilled circles) appear simultaneously both in the ($7^19^1$, 0, $J$) and ($7^2$, 2, $J-1$) branches, and must be distinguished by their eigenstate indices.

## 7. Parameters obtained

A summary of the data used in the fit is given in Tables 2 and 3. Data newly measured or reported in this work are specified in Section 3. The infrared data are listed in Table S1

of the electronic supplementary information, the hot-band transitions are listed in Table S2, and the millimeter/submillimeter wave transitions are listed in Tables S3 and S4. In addition to this data, we have included the rotational transitions in the $8^1$ and $6^1$ states previously used in [16] in Table S1 and high precision laser saturated IR data for the $\nu_8$ and $\nu_6$ bands obtained by Landsberg et al. [17] in Table S5. The submillimeter transitions from the Cologne laboratory, used also in Ref. [4], are given in Table S6, and all earlier measurements are listed in Table S7. All of these transitions were weighted according to the inverse square of their accuracies, which were estimated to be 0.0005 $cm^{-1}$ for all FTIR measurements, 0.25 MHz for laser saturated data, 0.04 MHz for a-type and 0.15 MHz for the weaker b-type rotational transitions in the excited vibrational states. A sample page selected from the MMW transitions assigned to the excited vibrational states is given in Table 10. It should be noted that the FASSST measurement yielded many new lines in the ground state, with higher quantum numbers than were included in [4]. Therefore, newly measured transitions in the ground state together with the microwave, MMW and SMMW rotational transitions used in Ref. [4] were also included in the fit. As a result, we have obtained not only parameters of the excited states but somewhat more accurate ground state parameters. The FIR data used in [4] were omitted in this fit; they did not contribute usefully to the determination of the parameters. The new parameters are included in Tables 4 and 5, where the ground state constants from [4] are given for comparison. No noticeable correlation between ground and excited state parameters could be detected.

The terms of the effective Hamiltonian (1), (2) were added gradually during a series of iterations of fitting and assigning, as sketched in Section 5. In successive iterations the significance of each new parameter was checked by requiring that its standard deviation be less than its value and that its inclusion improved significantly the agreement between observed and calculated transition frequencies. Finally, to reproduce all transitions used in the fit, 105 interaction terms were required in the Hamiltonian, coupling the seven excited vibrational states. The smallest ratio of the absolute value of a parameter to its standard deviation is 3.5 for the $[0,0,2,-]$ parameter between the $7^2$ and $7^19^1$ states.

A careful perusal of the set of the parameters determined in this work offers the possibility to make definite conclusions as to the principal interactions between the vibrational states under investigation. From another perspective, it is possible to determine those properties of the parameters which depend to a greater extent on the chosen form of the effective Hamiltonian than on properties of the molecule. The first observation in this respect is that because of the use of an effective Hamiltonian which is not reduced, there is a strong correlation between some parameters which leads to excessively high indeterminacies in their values. Therefore, the quoted number of significant figures in the parameters is not determined by their standard errors, but reflects the number of significant figures required to reproduce accurately the transition frequencies. Most constants, in the absence of correlation, would have much smaller standard errors with such a large amount of experimental data. Moreover, strong correlations lead not only to less accuracy of the parameters but also to distortions of their values. Owing to this fact, many parameters listed in Tables 4 and 5 must be considered as effective parameters. Despite this, 219 parameters predict the frequencies of more than 28,000 mm wave and infrared transitions and in fact describe all observed perturbations in the spectra, examples of which are presented in Section 6.

Let us begin with a discussion of the parameters of the diagonal blocks. It can be seen in Table 4 that there are no centrifugal distortion parameters with orders higher than expected. This indicates a sufficiently full accounting of the interactions. The quartic, sextic and even the octic parameters in the excited vibrational states have the same order of magnitude as in the ground state.

It is well known that quartic centrifugal distortion parameters should be almost independent of vibrational state. For the $7^2$, $7^19^1$ and $9^2$ states this assertion is not entirely fulfilled. For these states the theoretical expressions for quartic parameters in the presence of interactions differ from the expressions for the ground state, while for the other states investigated here they are the same in both cases. The difference can be accounted for by the fact that the operators of the form $q_7\hat{J}_\alpha\hat{J}_\beta$ and $q_9\hat{J}_\alpha\hat{J}_\beta$ in the rovibrational Hamiltonian, in the case of isolated vibrational states, contribute to the quartic centrifugal distortion parameters of the effective Hamiltonian, but in the presence of interactions that are explicitly treated, they are in the off-diagonal blocks. In the present case these operators are in the off-diagonal blocks connecting the $7^2$, $7^19^1$ and $9^2$ states. In general, all quartic centrifugal distortion parameters in the excited states are close to their respective values in the ground state, which indicates an acceptable quality of the fitting. The only exception is the $\delta_k$ parameter for the $6^1$ state. An imbalance of the quartic centrifugal distortion parameters may be caused by one of three reasons: Either the values of the parameters by definition cannot coincide with the ground state parameters, as is the case for the $7^2$, $7^19^1$ and $9^2$ states, or there are too few interaction terms, so that some interaction is not represented, or there is a redundancy among the interaction terms leading to high correlations and distortion of the values, as discussed above. In the latter case the magnitude of their 'distortion' can be qualitatively estimated from the average of each corresponding parameter over all interacting vibrational states. If the distortions are moderate, this average for all of the centrifugal distortion constants should be close to the corresponding values in the ground state. In this case the parameters may be regarded as acceptable. As can be seen from Table 11, the values of the quartic centrifugal distortion parameters averaged over the seven investigated vibrational states are close to the ground state values.

The dominant contribution to the interactions between the states is given by the parameters having indexes $[n,q,r,s] = [0,0,0,+]$, $[0,1,0,+]$, $[0,0,1,+]$ and $[0,0,1,-]$, which correspond to the Fermi and a-, b- and c- type first-order Coriolis

Table 10
Rotational transitions $^{a}R(14)_{0,1}$ in the seven excited states (MHz)

| Frequency | $J$ | $K_a$ | $K_c$ | O–C |
|---|---|---|---|---|
| $5^1$ | | | | |
| 323,266.10 | 14 | 0 | 14 | 0.01 |
| 320,300.70 | 14 | 1 | 14 | 0.02 |
| 341,562.71 | 14 | 1 | 13 | −0.04 |
| 332,285.33 | 14 | 2 | 13 | 0.03 |
| 343,638.69 | 14 | 2 | 12 | −0.01 |
| 335,741.54 | 14 | 3 | 12 | 0.02 |
| 337,481.89 | 14 | 3 | 11 | −0.01 |
| 335,399.65 | 14 | 4 | 11 | 0.08 |
| 335,627.39 | 14 | 4 | 10 | −0.11 |
| 335,032.53 | 14 | 5 | 9 | 0.00 |
| 335,889.69 | 14 | 5 | 10 | 0.06 |
| 334,356.00 | 14 | 6 | 9 | 0.00 |
| 334,358.09 | 14 | 6 | 8 | 0.01 |
| 332,282.66 | 14 | 7 | 8 | 0.00 |
| 332,289.80 | 14 | 7 | 7 | 0.02 |
| 338,871.58 | 14 | 8 | 6 | 0.04 |
| 338,871.58 | 14 | 8 | 7 | −0.03 |
| 336,946.85 | 14 | 9 | 5 | 0.00 |
| 336,946.85 | 14 | 9 | 6 | 0.00 |
| 336,318.09 | 14 | 10 | 4 | 0.07 |
| 336,318.09 | 14 | 10 | 5 | 0.07 |
| 336,016.43 | 14 | 11 | 3 | 0.03 |
| 336,016.43 | 14 | 11 | 4 | 0.03 |
| 335,905.46 | 14 | 12 | 3 | 0.00 |
| 335,905.46 | 14 | 12 | 2 | 0.00 |
| 335,789.73 | 14 | 13 | 1 | −0.04 |
| 335,789.73 | 14 | 13 | 2 | −0.04 |
| $7^2$ | | | | |
| 322,720.73 | 14 | 0 | 14 | 0.01 |
| 319,670.12 | 14 | 1 | 14 | −0.04 |
| 337,487.60 | 14 | 1 | 13 | −0.04 |
| 327,866.81 | 14 | 2 | 13 | 0.06 |
| 339,367.14 | 14 | 2 | 12 | −0.01 |
| 331,470.14 | 14 | 3 | 12 | 0.01 |
| 335,335.73 | 14 | 3 | 11 | 0.04 |
| 334,719.59 | 14 | 4 | 10 | 0.03 |
| 333,606.79 | 14 | 5 | 9 | 0.02 |
| 334,222.63 | 14 | 5 | 10 | 0.03 |
| 341,670.29 | 14 | 6 | 9 | −0.09 |
| 334,721.63 | 14 | 7 | 8 | 0.10 |
| 334,721.63 | 14 | 7 | 7 | 0.05 |
| 336,109.81 | 14 | 9 | 5 | 0.04 |
| 336,109.81 | 14 | 9 | 6 | 0.04 |
| 336,042.78 | 14 | 10 | 4 | 0.03 |
| 336,042.78 | 14 | 10 | 5 | 0.03 |
| 336,031.13 | 14 | 11 | 4 | −0.09 |
| 336,031.13 | 14 | 11 | 3 | −0.09 |
| 336,098.09 | 14 | 13 | 2 | −0.01 |
| 336,098.09 | 14 | 13 | 1 | −0.01 |
| 336,155.01 | 14 | 14 | 0 | 0.04 |
| 336,155.01 | 14 | 14 | 1 | 0.04 |
| $9^2$ | | | | |
| 323,632.16 | 14 | 0 | 14 | 0.00 |
| 320,053.30 | 14 | 1 | 14 | 0.01 |
| 343,417.42 | 14 | 1 | 13 | −0.08 |
| 333,635.95 | 14 | 2 | 13 | −0.01 |
| 346,160.29 | 14 | 2 | 12 | −0.04 |
| 337,663.62 | 14 | 3 | 12 | −0.02 |
| 339,682.02 | 14 | 3 | 11 | −0.01 |
| 337,759.19 | 14 | 4 | 11 | −0.09 |
| 337,863.14 | 14 | 4 | 10 | 0.01 |
| 337,997.84 | 14 | 5 | 10 | −0.01 |
| 338,000.38 | 14 | 5 | 9 | 0.02 |
| 338,084.18[a] | 14 | 6 | 9 | 0.12 |
| 338,084.18[a] | 14 | 6 | 8 | 0.00 |
| 335,011.53[a] | 14 | 7 | 7 | 0.19 |
| 335,011.53[a] | 14 | 7 | 8 | −0.08 |
| 335,759.26 | 14 | 8 | 7 | −0.02 |
| 335,759.26 | 14 | 8 | 6 | −0.02 |
| 335,975.37 | 14 | 9 | 6 | 0.04 |
| 335,975.37 | 14 | 9 | 5 | 0.04 |
| 336,130.92 | 14 | 11 | 4 | −0.01 |
| 336,130.92 | 14 | 11 | 3 | −0.01 |
| 336,181.31 | 14 | 12 | 2 | 0.04 |
| 336,181.31 | 14 | 12 | 3 | 0.04 |
| 336,214.57 | 14 | 13 | 2 | 0.07 |
| 336,214.57 | 14 | 13 | 1 | 0.07 |
| 336,223.90 | 14 | 14 | 0 | −0.06 |
| 336,223.90 | 14 | 14 | 1 | −0.06 |
| $4^1$ | | | | |
| 324,426.50 | 14 | 0 | 14 | 0.01 |
| 321,567.76 | 14 | 1 | 14 | −0.07 |
| 344,536.33 | 14 | 1 | 13 | −0.01 |
| 334,709.98 | 14 | 2 | 13 | 0.01 |
| 347,692.62 | 14 | 2 | 12 | −0.03 |
| 338,843.54 | 14 | 3 | 12 | −0.02 |
| 341,042.33 | 14 | 3 | 11 | −0.02 |
| 338,802.55 | 14 | 4 | 11 | −0.03 |
| 338,919.97 | 14 | 4 | 10 | −0.03 |
| 338433.93 | 14 | 5 | 10 | −0.03 |
| 338437.03 | 14 | 5 | 9 | −0.03 |
| 338,225.39[a] | 14 | 6 | 9 | −0.08 |
| 338,225.39[a] | 14 | 6 | 8 | −0.12 |
| 338,151.69 | 14 | 7 | 8 | −0.03 |
| 338,151.69 | 14 | 7 | 7 | −0.03 |
| 338,080.64 | 14 | 9 | 5 | 0.03 |
| 338,080.64 | 14 | 9 | 6 | 0.03 |
| 338,102.21 | 14 | 10 | 4 | −0.10 |
| 338,102.21 | 14 | 10 | 5 | −0.10 |
| 338,149.16 | 14 | 11 | 3 | −0.02 |
| 338,149.16 | 14 | 11 | 4 | −0.02 |
| $6^1$ | | | | |
| 322,537.17 | 14 | 0 | 14 | 0.01 |
| 319,598.73 | 14 | 1 | 14 | 0.00 |
| 342,254.10 | 14 | 1 | 13 | −0.01 |
| 345,050.98 | 14 | 2 | 12 | 0.03 |
| 336,471.79 | 14 | 3 | 12 | 0.07 |
| 338,516.65 | 14 | 3 | 11 | 0.00 |
| 336,415.25 | 14 | 4 | 11 | 0.12 |
| 336,521.07 | 14 | 4 | 10 | −0.01 |
| 336,056.02 | 14 | 5 | 10 | 0.04 |
| 336,058.72 | 14 | 5 | 9 | 0.03 |
| 335,862.21 | 14 | 6 | 9 | 0.06 |
| 335,862.21 | 14 | 6 | 8 | 0.02 |
| 335,770.05 | 14 | 7 | 8 | 0.03 |
| 335,770.05 | 14 | 7 | 7 | 0.03 |
| 335,710.78 | 14 | 8 | 7 | 0.00 |
| 335,710.78 | 14 | 8 | 6 | 0.00 |
| 335,700.92 | 14 | 9 | 6 | 0.01 |
| 335,700.92 | 14 | 9 | 5 | 0.01 |
| 335,714.91 | 14 | 10 | 4 | 0.09 |
| 335,714.91 | 14 | 10 | 5 | 0.05 |
| 335,732.87 | 14 | 11 | 3 | −0.01 |
| 335,732.87 | 14 | 11 | 4 | −0.01 |
| 335,766.99 | 14 | 12 | 3 | −0.02 |
| 335,766.99 | 14 | 12 | 2 | −0.02 |
| 335,809.29 | 14 | 13 | 1 | −0.04 |
| 335,809.29 | 14 | 13 | 2 | −0.04 |

Table 10 (*continued*)

| Frequency | $J$ | $K_a$ | $K_c$ | O–C |
|---|---|---|---|---|
| $7^1 9^1$ | | | | |
| 325,746.11 | 14 | 0 | 14 | −0.03 |
| 325,663.33 | 14 | 1 | 14 | −0.03 |
| 348,306.96 | 14 | 1 | 13 | 0.04 |
| 336,385.18 | 14 | 2 | 13 | 0.07 |
| 348,246.92 | 14 | 2 | 12 | −0.01 |
| 341,054.33 | 14 | 3 | 12 | −0.02 |
| 342,960.61 | 14 | 3 | 11 | −0.04 |
| 341,578.08 | 14 | 4 | 11 | −0.05 |
| 341,613.92 | 14 | 4 | 10 | −0.03 |
| 334,548.43 | 14 | 5 | 10 | −0.04 |
| 334,549.50 | 14 | 5 | 9 | 0.00 |
| 333,872.26[a] | 14 | 6 | 9 | 0.12 |
| 333,872.26[a] | 14 | 6 | 8 | 0.03 |
| 333,592.03 | 14 | 7 | 8 | 0.09 |
| 333,592.03 | 14 | 7 | 7 | −0.06 |
| 336,929.92 | 14 | 9 | 5 | 0.01 |
| 336,929.92 | 14 | 9 | 6 | 0.01 |
| 336,892.49 | 14 | 10 | 4 | −0.04 |
| 336,892.49 | 14 | 10 | 5 | −0.04 |
| 336,943.17 | 14 | 11 | 4 | −0.09 |
| 336,943.17 | 14 | 11 | 3 | −0.09 |
| 337,129.73 | 14 | 13 | 2 | 0.03 |
| 337,129.73 | 14 | 13 | 1 | 0.03 |
| 337,253.96 | 14 | 14 | 1 | −0.05 |
| 337,253.96 | 14 | 14 | 0 | −0.05 |
| $8^1$ | | | | |
| 324,227.58 | 14 | 0 | 14 | 0.01 |
| 321,299.01 | 14 | 1 | 14 | −0.06 |
| 343,097.70 | 14 | 1 | 13 | −0.02 |
| 333,666.03 | 14 | 2 | 13 | 0.01 |
| 345,530.89 | 14 | 2 | 12 | −0.03 |
| 337,393.72 | 14 | 3 | 12 | −0.03 |
| 339,266.13 | 14 | 3 | 11 | −0.01 |
| 337,320.15 | 14 | 4 | 11 | −0.03 |
| 337,414.66 | 14 | 4 | 10 | −0.03 |
| 336,976.74 | 14 | 5 | 10 | −0.04 |
| 336,979.10 | 14 | 5 | 9 | −0.02 |
| 336,788.21[a] | 14 | 6 | 8 | 0.00 |
| 336,788.21[a] | 14 | 6 | 9 | −0.09 |
| 336,689.52 | 14 | 7 | 8 | 0.02 |
| 336,689.52 | 14 | 7 | 7 | 0.00 |
| 336,638.39 | 14 | 8 | 7 | −0.01 |
| 336,638.39 | 14 | 8 | 6 | −0.01 |
| 336,611.92 | 14 | 9 | 6 | −0.01 |
| 336,611.92 | 14 | 9 | 5 | −0.01 |
| 336,624.97 | 14 | 10 | 4 | 0.01 |
| 336,624.97 | 14 | 10 | 5 | 0.01 |
| 336,634.73 | 14 | 11 | 4 | 0.03 |
| 336,634.73 | 14 | 11 | 3 | 0.03 |
| 336,657.80 | 14 | 12 | 2 | 0.02 |
| 336,657.80 | 14 | 12 | 3 | 0.02 |
| 336,729.31 | 14 | 14 | 1 | −0.10 |
| 336,729.31 | 14 | 14 | 0 | −0.10 |

Only lower state quantum numbers of the transitions are given.
[a] Not used in the fit.

interactions, respectively. A Fermi interaction has a strong correlation with the relevant band origins. It occurs between states of the same symmetry and, if the sum of the differences of the vibrational quantum numbers of the states is three, is

Table 11
Comparison of the quartic centrifugal distortion parameters averaged over all excited states and ground state values of HCOOH (kHz)

| | Ground state | Averaged |
|---|---|---|
| $\Delta_J$ | 9.99462 | 9.95801 |
| $\Delta_{JK}$ | −86.2176 | −86.2823 |
| $\Delta_K$ | 1702.292 | 1736.334 |
| $\delta_J$ | 1.948585 | 1.944057 |
| $\delta_K$ | 42.7739 | 41.8477 |

determined by the corresponding cubic force field constants. As can be seen from Table 5, an appreciable first order Fermi interaction ([0,0,0,+] parameter) was found between the four pairs of states $5^1/7^2$, $5^1/9^2$, $7^2/6^1$ and $9^2/4^1$, i.e. all five states of $A'$ symmetry are affected by such interactions. The $8^1$ and $7^1 9^1$ states of $A''$ symmetry barely interact. Because of this the accuracies of the $8^1$ and $7^1 9^1$ unperturbed band centers are five orders of magnitude higher than those of the five $A'$ states. The largest Fermi coupling constant of 41.5 $cm^{-1}$ couples the $5^1$ and $9^2$ state, and as was mentioned above, it is responsible for the anomalously high intensity of the $2\nu_9$ band. The value determined more than confirms the initial estimate of 30 $cm^{-1}$.

In Table 12 we compare the band origins obtained here for the $7^2$, $7^1 9^1$ and $9^2$ states with their values estimated using the published fundamental band centers. Due to vibrational anharmonicity the unperturbed 'observed' band centers of such combination or overtone states should be somewhat less than the sum of the singly excited constituents. This inequality, as can be seen from Table 12, holds only for the $2\nu_7$ band. For the other two bands this relation is reversed. This means that their values, in particular, due to the redundancies and high correlations, have to be considered as effective parameters.

First-order Coriolis interaction parameters are correlated with the rotational parameters, and the magnitude of the correlation is inversely proportional to the strength of the interaction. Naturally, the magnitude of this correlation depends on the value of the interaction coefficient and the difference of the energies of the interacting levels. If centrifugal distortion corrections to the first-order Coriolis terms are chosen poorly, strong correlations and distortion of the parameters' values can appear. From this point of view, it is helpful to analyze the Coriolis coupling parameters between the states $7^2/7^1 9^1$, $9^2/7^1 9^1$ and $6^1/8^1$, and also the rotational parameters for these states. Theoretically, a- and b-type parameters of the Coriolis interactions $7^2/7^1 9^1$ and $9^2/7^1 9^1$ should be, according to the expressions (6) and (7), opposite in sign and $\sqrt{2}$ times more than the corresponding coupling of the $7^1/9^1$ states. In Table 13 the Coriolis interaction parameters obtained in the present work and their estimates from the

Table 12
Estimated and obtained $2\nu_7$, $\nu_7+\nu_9$ and $2\nu_9$ band centers ($cm^{-1}$)

| Band | $\nu_i+\nu_j$ from Ref. [22] | $\nu_0$ (Table 4) | $\nu_0-(\nu_i+\nu_j)$ |
|---|---|---|---|
| $2\nu_7$ | 1252.3 | 1249.0 | −3.3 |
| $\nu_7+\nu_9$ | 1266.9 | 1268.7 | 1.8 |
| $2\nu_9$ | 1281.4 | 1288.4 | 7.0 |

Table 13
Comparison of Coriolis coupling parameters determined for HCOOH (MHz)

| Interacting states | Parameter [n,q,r,s] | Present work | Estimated or determined previously | Δ[a] |
|---|---|---|---|---|
| $7^2$–$7^1 9^1$ | [010+] | 48,800 | 44,567[b] | 8.7 |
| | [001+] | 7315 | 5568[b] | 23.9 |
| $9^2$–$7^1 9^1$ | [010+] | −35,624 | −44,567[b] | −25.1 |
| | [001+] | −4518 | −5568[b] | −23.2 |
| $6^1$–$8^1$ | [010+] | 11,305 | 23,234[c] | −105.5 |
| | [001+] | 1503 | 229[c] | 84.8 |

[a] $\Delta = ([n,q,r,s]_{\text{Present}} - [n,q,r,s]_{\text{Estimated}})/[n,q,r,s]_{\text{Present}}$ %.
[b] Coriolis coupling parameters [010+] = 31,514 and [001+] = 3937 MHz for $7^1$–$9^1$ interacting states from Ref. [22] multiplied by $\sqrt{2}$.
[c] From Ref. [16].

results of [22] are gathered for comparison. It is seen that the parameters corresponding to the $7^2/7^1 9^1$ pair of states match reasonably well with initial estimates. In particular, the signs of the Coriolis coupling parameters of the $7^2/7^1 9^1$ and $9^2/7^1 9^1$ states are opposite, as expected. However, the parameters for the $9^2/7^1 9^1$ states are significantly less than the predicted ones. This can be explained by the Fermi interaction between the $9^2$ and $5^1$ states. In the rotational eigenfunctions of the $9^2$ state, due to this interaction, there are contributions of the basis functions of the $5^1$ state, in the ratio 2:1 (Fig. 13). Since the matrix element (6) which in the main determines the value of the first order Coriolis coupling parameters does not depend on the $5^1$ state component, the ratio of the absolute values of the parameters between the $7^2/7^1 9^1$ and $9^2/7^1 9^1$ pairs of states should be equal to 1.5. The actual ratios of the a- and b-type Coriolis parameters for these pairs of interacting states are 1.37 and 1.62, which are reasonably close to 1.5.

The parameters of the Coriolis interaction between the $6^1$ and $8^1$ states determined in the present study differ significantly from those calculated in earlier work [16]. The previous values were close to those computed from the harmonic force field and the known structure of the molecule, and therefore we consider them more reliable, and the parameters determined in the present study should be treated as effective. They are strongly correlated with the rotational constants of the $6^1$ and $8^1$ states, since the interaction is not strong, and with higher order interaction parameters. The effect of the Coriolis interaction between the $6^1$ and $8^1$ states is an order of magnitude less than for the $7^1$ and $9^1$ states, and much less than between the $7^2/7^1 9^1$ or $9^2/7^1 9^1$ states, primarily due to the larger difference of vibrational energies. The considerable difference of the magnitudes of the interactions is proved by the fact that in the first investigations dealing with the study of pure rotational transitions in the $6^1$ and $8^1$ vibrational states [19,20], it was possible to use a model of isolated vibrational states to describe the observed transitions with relatively low $J$ and $K_a$ values. To study the rotational transitions in the $7^1$ and $9^1$ states it was necessary from the very outset to invoke a model of interacting vibrational states [23,24].

A similar picture exists for the rotational parameters of the $7^2$, $7^1 9^1$ and $9^2$ states, on the one hand, and of the $6^1$ and $8^1$ states, on the other hand. While the values of the rotational parameters of the $7^2$, $7^1 9^1$ and $9^2$ states correspond to their estimates obtained from the parameters of the lower vibrational states, as shown in Table 14, the rotational constants of the $6^1$ and $8^1$ states from the present work and in [16] differ strongly, as shown in Table 15.

Some of the correlations between the spectroscopic constants are probably caused by a non-optimal choice of the set of parameters. Thus, for example, to bring into agreement the calculated and observed wavenumbers of the transitions with high $K_a$ in the $\nu_6$ band, it was necessary to incorporate additional interaction parameters which were not in the previous analysis of those states [16]. It is not surprising that these newly added parameters could distort levels with lower $K_a$ values. Therefore, further parameters were necessary to compensate the negative influence of the first additional parameters on the low $K_a$ levels. These parameters can be called 'compensatory'. If the first set of additional parameters

Table 14
Vibrational dependence of the rotational parameters of HCOOH (MHz)

| Parameter | $7^1$ | $R_{7^1} - R_{gs}$ | $7^2$ | $R_{7^2} - R_{gs}$ | $2(R_{7^1} - R_{gs})$ |
|---|---|---|---|---|---|
| $A$ | 77,755.3 | 243.1 | 77,975.2 | 463.0 | 486.2 |
| $B$ | 12,034.7 | −20.4 | 12,064.5 | 9.4 | −40.7 |
| $C$ | 10,395.0 | −21.1 | 10,308.1 | −108.0 | −42.3 |
| $(B+C)/2$ | 11,214.8 | −20.8 | 11,186.3 | −49.3 | −41.5 |
| | $9^1$ | $R_{9^1} - R_{gs}$ | $7^1 9^1$ | $R_{7^1 9^1} - R_{gs}$ | $R_{7^1} + R_{9^1} - 2R_{gs}$ |
| $A$ | 77,685.0 | 172.8 | 78,056.7 | 544.4 | 416.0 |
| $B$ | 12,006.9 | −48.2 | 11,928.1 | −127.0 | −68.6 |
| $C$ | 10,405.3 | −10.8 | 10,380.1 | −36.0 | −32.0 |
| $(B+C)/2$ | 11,206.1 | −29.5 | 11,154.1 | −81.5 | −50.3 |
| | | | $9^2$ | $R_{9^2} - R_{gs}$ | $2(R_{9^1} - R_{gs})$ |
| $A$ | | | 77,885.0 | 373.8 | 345.6 |
| $B$ | | | 11,966.4 | −88.7 | −96.4 |
| $C$ | | | 10,401.3 | −14.9 | −21.7 |
| $(B+C)/2$ | | | 11,183.8 | −51.8 | −59.0 |

Rotational parameters for $7^1$ and $9^1$ states were taken from Ref. [22].

Table 15
Comparison of the rotational parameters of HCOOH in the $6^1$ and $8^1$ states from this work and from Ref. [16]

| Parameter | $6^1$ | | $8^1$ | |
|---|---|---|---|---|
| | This work | Ref. [16] | This work | Ref. [16] |
| *A* | 77803.26 | 77601.13 | 78044.90 | 76976.49 |
| *B* | 12016.53 | 12003.10 | 12063.27 | 12001.72 |
| *C* | 10416.38 | 10352.04 | 10418.77 | 10419.62 |

Rotational parameters are in MHz.

is not chosen optimally, the number of compensatory parameters can be too large. From this it follows that a strong correlation can arise. This situation differs from that of adding higher order centrifugal distortion terms, because the interaction contributions depend not only upon the values of quantum numbers but also on the variation of the energy differences between interacting levels in a progression of quantum numbers. In Fig. 15, for example, one sees a highly non-monotonic behavior of the residuals as a function of $K_a$. The rotational transitions, and the b-type transitions in particular, are especially sensitive to the higher order Coriolis interaction terms. As can be seen in Fig. 13, the $6^1$ state is only weakly perturbed. Nevertheless, the number of interaction parameters of this state with others required for the fit is rather large: 7 with the $5^1$ state, 8 with $7^1$, 7 with $9^2$, 4 with $7^19^1$, 2 with $4^1$, and 10 with $8^1$; in all 38 interaction parameters. However, such a large number of parameters may not only reflect redundancy in the set of parameters, but may also represent actual fine interactions which are determined by high precision rotational transitions.

The most strongly interacting states are the $7^2$ and $7^19^1$ states. It requires 14 parameters to describe their interaction. Remarkably, the $4^1$ and $8^1$ states, which are separated by more than 300 $cm^{-1}$, also show a mutual influence through first-order a- and b-types Coriolis interactions. For some pairs of vibrational states, in particular the $9^2/8^1$ and $4^1/6^1$ pairs, the essential interactions are high order interactions. The choice of these parameters is determined by the difference $\Delta K_a$ of nearly coincident interacting levels, which coincides with the *r* indices of the interaction terms.

In spite of the strong correlations in the set of the parameters presented here, with slight distortions of some values, the analysis may be considered complete according to several criteria: First, it reproduces all transitions used in the fit, both infrared and millimeter wave, with accuracies close to the uncertainties of the measurements (Tables 2 and 3). Second, the number of the assigned FTIR transitions and maximal values of *J* and $K_a$ quantum numbers for the strongest bands in that region, the $\nu_6$ and $\nu_5$ bands, reach the values estimated in Section 1, indicating that all observable interactions have been taken into account.

## Acknowledgements

We wish to thank Dr Jean Demaison for his advice in a very initial stage of this work. The FASSST millimeter wave work at The Ohio State University was supported by grants from NASA and ARO. OIB acknowledges the financial support of the Academy of Finland.

## Supplementary data

Supplementary data associated with this article can be found, in the online version, at doi:10.1016/j.molstruc.2006.02.052.

## References

[1] E. Willemot, D. Dangoisse, N. Monnanteuil, J. Bellet, J. Phys. Chem. Data 9 (1980) 59.
[2] O.I. Baskakov, M.V. Moskienko, S.F. Duybko, Zh. Priklad. Spektrosk. 23 (1975) 692 (in Russian).
[3] J. Vander Auwera, J. Mol. Spectrosc. (1992) 155.
[4] M. Winnewisser, B.P. Winnewisser, M. Stein, M. Birk, G. Wagner, G. Winnewisser, K.M.T. Yamada, S. Belov, O.I. Baskakov, J. Mol. Spectrosc. 216 (2002) 259.
[5] I.C. Hisatsune, J. Heicklen, Can. J. Spectrosc. 18 (1973) 135.
[6] I.D. Reva, A.M. Plokhotnichenko, E.D. Radchenko, G.G. Sheina, Yu.P. Blagoi, Spectrochim. Acta, A 50 (1994) 1107.
[7] R.C. Milliken, K.S. Pitzer, J. Chem. Phys. 27 (1957) 1305.
[8] R.L. Redington, J. Mol. Spectrosc. 65 (1977) 171.
[9] D. Hurtmans, F. Herregods, M. Herman, J. Lievin, J. Chem. Phys. 113 (2000) 1535.
[10] M. Freytes, D. Hurtmans, S. Kassi, J. Lievin, J. Vander Auwera, A. Campargue, M. Herman, Chem. Phys. 283 (2002) 47.
[11] D. Dangoisse, P. Glorieux, in: K.J. Button, M. Inguscio, F. Strumia (Eds.), Reviews of Infrared and Millimeter Waves, vol. 2, Plenum Press, New York, London, 1984, p. 429.
[12] M. Inguscio, G. Moruzzi, K.M. Evenson, D.A. Jennings, J. Appl. Phys. 60 (1986) R161.
[13] A. Perrin, C.P. Rinsland, A. Goldman, J. Geophys. Res. D104 (1999) 18661.
[14] R.E. Bumgarner, J.-I. Choe, S.G. Kukolich, R.J. Butcher, J. Mol. Spectrosc. 132 (1988) 261.
[15] T.L. Tan, K.L. Goh, P.P. Ong, H.H. Teo, J. Mol. Spectrosc. 202 (2000) 194.
[16] O.I. Baskakov, J. Demaison, J. Mol. Spectrosc. 211 (2002) 262.
[17] B.M. Landsberg, D. Crocker, R.J. Butcher, J. Mol. Spectrosc. 92 (1982) 67.
[18] H.-T. Man, R. Butcher, J. Mol. Spectrosc. 107 (1984) 284.
[19] E. Willemot, D. Dangoisse, J. Bellet, J. Mol. Spectrosc. 77 (1979) 161.
[20] O.I. Baskakov, S.F. Dyubko, M.V. Moskienko, L.D. Fesenko, Sov. J. Quantum Electron. 7 (1977) 445.
[21] J.C. Deroche, J. Kauppinen, E. Kyrö, J. Mol. Spectrosc. 78 (1979) 379.
[22] A. Perrin, J.-M. Flaud, B. Bakri, J. Demaison, O. Baskakov, S.V. Sirota, M. Herman, J. Vander Auwera, J. Mol. Spectrosc. 216 (2002) 203.
[23] E. Willemot, D. Dangoisse, J. Bellet, J. Mol. Spectrosc. 73 (1978) 96.
[24] E. Willemot, J. Mol. Spectrosc. 120 (1986) 246.
[25] H. Kuze, T. Amano, T. Shimizu, J. Chem. Phys. 77 (1982) 714.
[26] W.H. Weber, P.D. Maker, J.W.C. Johns, E. Weinberger, J. Mol. Spectrosc. 121 (1987) 243.
[27] K.L. Goh, P.P. Ong, T.L. Tan, Spectrochim. Acta A55 (1999) 2609.
[28] K.L. Goh, P.P. Ong, T.L. Tan, W.F. Wang, H.H. Teo, J. Mol. Spectrosc. 190 (1998) 125.
[29] K.L. Goh, P.P. Ong, T.L. Tan, H.H. Teo, W.K. Wang, J. Mol. Spectrosc. 191 (1998) 343.
[30] K.L. Goh, P.P. Ong, H.H. Teo, T.L. Tan, J. Mol. Spectrosc. 197 (1999) 322.
[31] P.P. Ong, K.L. Goh, H.H. Teo, J. Mol. Spectrosc. 194 (1999) 203.
[32] T.L. Tan, K.L. Goh, P.P. Ong, H.H. Teo, J. Mol. Spectrosc. 198 (1999) 110.
[33] T.L. Tan, K.L. Goh, P.P. Ong, H.H. Teo, J. Mol. Spectrosc. 199 (1999) 387.

[34] K.L. Goh, P.P. Ong, T.L. Tan, H.H. Teo, Spectrochim. Acta A55 (1999) 1309.
[35] L. Nemes, A.R.W. McKellar, J.W.C. Johns, J. Opt. Soc. Am. B4 (1987) 1165.
[36] O.I. Baskakov, H. Burger, W. Jerzembeck, J. Mol. Spectrosc. 193 (1999) 33.
[37] O.I. Baskakov, J. Lohilahti, V.-M. Horneman, J. Mol. Spectrosc. 219 (2003) 191.
[38] O.I. Baskakov, S. Alanko, M. Koivusaari, J. Mol. Spectrosc. 198 (1999) 40.
[39] O.I. Baskakov, J. Mol. Spectrosc. 213 (2002) 1.
[40] J.E. Bertie, K.H. Michaelian, J. Chem. Phys. 76 (1982) 886.
[41] T. Ahonen, P. Karhu, V.-M. Horneman in: J.M. Flaud, M. Quack, A. Trombetti, G. Duxbury (Eds.). Proceedings of the Fifteenth Colloquium on High Resolution Molecular Spectroscopy, University of Strathclyde, Glasgow, Scotland, 7–11 September 1997, Unversity of Strathclyde, Glasgow, Scotland, 1997, p. 200.
[42] P. Karhu, T. Ahonen, V.-M. Horneman, R. Anttila, http://physics.oulu.fi/irspe/Sivut/cell40-2002.pdf
[43] G. Guelachvili, K. Narahari Rao, Handbook of Infrared Standards, Academic Press, Orlando, FL, 1986.
[44] G. Guelachvili, D. Hausamann, J.W.C. Johns, J. Kauppinen, Q. Kou, A.G. Maki, K. Narahari Rao, R.A. Toth, W. Urban, A. Valentin, J. Vergès, M. Birk, G. Wagner, M.H. Wappelhorst, J.S. Wells, B.P. Winnewisser, M. Winnewisser, C.J. Bordé, J.W. Brault, L.R. Brown, B. Carli, A.R.H. Cole, K.M. Evenson, A. Fayt, Pure Appl. Chem. 68 (1996) 193.
[45] V.V. Ilyushin, E.A. Alekseev, S.F. Dyubko, O.I. Baskakov, J. Mol. Spectrosc. 195 (1999) 246.
[46] D.T. Petkie, T.M. Goyette, R.A.P. Bettens, S.P. Belov, S. Albert, P. Helminger, F.C. De Lucia, Rev. Sci. Instrum. 68 (1997) 1675.
[47] S. Albert, D.T. Petkie, R.A.P. Bettens, S.P. Belov, F.C. De Lucia, Anal. Chem. News Features 70 (1998) 719A.
[48] I. Medvedev, M. Winnewisser, F.C. DeLucia, E. Herbst, E. Li, L.P. Leong, R.P.A. Bettens, E. Białkowska-Jaworska, O. Desyatnyk, L. Pszczółkoski, Z. Kisiel, Astrophys. J. Suppl. 148 (2003) 593.
[49] I. Medvedev, M. Winnewisser, F.C. De Lucia, E. Herbst, E. Białkowska-Jaworska, L. Pszczółkoski, Z. Kisiel, J. Mol. Spectrosc. 228 (2004) 314.
[50] I.R. Medvedev, Dissertation, The Ohio State University, 2005.
[51] V.I. Perevalov, Vl.G. Tyuterev, Optika i Spektroskopija 52 (1982) 644 (in Russian).
[52] V.I. Perevalov, Vl.G. Tyuterev, J. Mol. Spectrosc. 96 (1982) 56.
[53] J.K.G. Watson, Mol. Phys. 100 (2002) 47.
[54] K. Yamada, M. Winnewisser, Z. Naturforsch. 30A (1975) 672.